Dynamic Process Model Validation and Control of the Amine Plant at CO₂ Technology Centre Mongstad

Rubén M. Montañés [1],* [ID], Nina E. Flø [2] and Lars O. Nord [1] [ID]

[1] Department of Energy and Process Engineering, NTNU—Norwegian University of Science and Technology, NO-7491 Trondheim, Norway; lars.nord@ntnu.no

[2] CO₂ Technology Center Mongstad, NO-5954 Mongstad, Norway; nflo@tcmda.no

* Correspondence: ruben.m.montanes@ntnu.no; Tel.: +47-73-5073722

Abstract: This paper presents a set of steady-state and transient data for dynamic process model validation of the chemical absorption process with monoethanolamine (MEA) for post-combustion CO₂ capture of exhaust gas from a natural gas-fired power plant. The data selection includes a wide range of steady-state operating conditions and transient tests. A dynamic process model developed in the open physical modeling language Modelica is validated. The model is utilized to evaluate the open-loop transient performance at different loads of the plant, showing that pilot plant main process variables respond more slowly at lower operating loads of the plant, to step changes in main process inputs and disturbances. The performance of four decentralized control structures is evaluated, for fast load change transient events. Manipulation of reboiler duty to control CO₂ capture ratio at the absorber's inlet and rich solvent flow rate to control the stripper bottom solvent temperature showed the best performance.

1. Introduction

Carbon capture and storage (CCS) is a group of technologies that can significantly contribute to the reduction of anthropogenic CO₂ emissions from thermal power generation and other carbon-intensive industries [1]. There are two commercial-scale coal-fired power plants with post-combustion CO₂ capture (PCC) using amines being operated today, at Boundary Dam in Canada [2] and at Petra Nova project at the Parish Power Station in the US [3]. These projects prove the technical feasibility of the technology at commercial scale. Among the different options and technologies for CO₂ capture in thermal power generation, post-combustion CO₂ capture with chemical absorption is considered the more mature technology that can contribute to significantly reducing the carbon intensity (kgCO₂/kWh_el) of fossil-fueled thermal power plants. In future energy systems with a high penetration of renewable energy sources, the variability in demand and generation will introduce a change in the operating patterns of thermal power generation plants, which will have to change operating conditions [4–6]; there will also be a higher frequency of significant transient events including load changes, and start-up and shut-down events [7,8]. In this regard, Boot-Handford et al.'s carbon capture and storage update 2014 concludes that the financial case for CCS requires that it operates in a flexible manner and that load-following ability is extremely important to the long-term economics [9].

Among the different features of flexible operation of power plants with CCS, an important aspect is the transient behavior of the system when varying operating conditions. This means that efficient operation and emissions and the related operational costs during transient operation will gain importance. However, the operational experience from commercial-scale power plants with post

combustion CO_2 capture is scarce and the published transient pilot plant data from test campaigns is limited. Therefore, there is a need for the development of dynamic process models. Dynamic process models can contribute to developing the learning curve for flexible operation of PCC plants. These tools can assist in evaluating the feasibility of flexible operation strategies as well as design process configurations and operational strategies that can lead to the reduction of operational costs and increased revenue during power plant operation. The study of the transient performance with dynamic process models can contribute to identifying process bottlenecks and ease the process scale-up.

Dynamic process models allow the study of the open-loop transient performance of the plant [10], the evaluation of different process configurations and designs [11], the development and implementation of optimal control strategies [12–20], as well as the study of the plant behavior under different operational flexibility scenarios [21,22]. In addition, the power plant and the PCC unit can be treated as an integrated system and dynamic process models can be utilized to analyze the response of the capture unit to changes that occur upstream in the power plant [12,15,19,23–25]. Furthermore, the operational flexibility of the PCC plant can be improved with plant design or using control strategies [26–29]. The core purpose of dynamic process models is to capture the time-dependent behavior of the process under transient conditions. However, the validation of dynamic process models with experiments and pilot plant data is necessary in order to assess the reliability of simulation results.

Kvamsdal et al. [30] developed a dynamic process model of a CO_2 absorber column and used steady-state data from a pilot plant to validate liquid temperature profiles, capture ratio % and rich loading. That work highlighted the necessity of building up a dynamic process model of the integrated system (including stripper, lean/rich heat exchanger, mixing tank and main process equipment), to understand the complexities of dynamic operation of the plant. Gaspar and Cormos [31] developed a dynamic process model of the absorber/desorber process and validated with steady-state plant data. Several publications are available, in which the models were validated only with steady-state pilot plant data [11,32–35]. Biliyok et al. [36] presented a dynamic model validation study where transient data was driven by decrease in solvent flow rate to the absorber, fluctuating concentration of CO_2 at absorber inlet and a varying absorber's feed flue gas stream temperature to the absorber. A dynamic process model developed in Modelica language was validated with transient data from the Esbjerg pilot plant by Åkesson et al. [37]. That data consisted of the transient performance after one step-change in flue gas mass flow rate. An extensive review work by Bui et al. [38] concluded that research efforts are required on producing transient pilot plant data.

More recent works have included validation of dynamic process models with transient plant data from pilot plants. A K-Spice model by Flø et al. was validated with pilot plant data from the Brindisi pilot plant [39]. Flø et al. [40] validated a dynamic process model of CO_2 absorption process, developed in Matlab, with steady-state and transient pilot plant data from the Gløshaugen (Norwegian University of Science and Technology (NTNU)/SINTEF) pilot plant. Van de Haar et al. [41] conducted dynamic process model validation of a dynamic process model in Modelica with transient data from a pilot plant located at the site of the coal-fired Maasvlakte power plant in the Netherlands. Gaspar et al. [42] conducted model validation with transient data from two step changes in flue gas volumetric flow rate from the Esbjerg pilot plant. Other works include the validation of equilibrium-based models such as that of Dutta et al. [43]; or the work by Chinen et al. [44] which conducted dynamic process model validation of a process model in Aspen Plus® with transient plant data from the National Carbon Capture Center (NCCC) in the US. Manaf et al. [45] developed a data-driven black box mathematical model, based on transient pilot plant data, by means of system identification. In addition, dynamic process models have been developed to study the transient behavior of the chemical absorption CO_2 capture process using piperazine (PZ) as chemical solvent [19,20]. It should be noted that the majority of work has been conducted for typical flue gas compositions from coal-based power plants with CO_2 concentration around 12 vol % [38].

From the literature review it can be concluded that dynamic process model validation is a challenging process due to:

- The scarce availability of transient or dynamic pilot plant data.
- Most available data is found from small-scale pilot plants. That has implications for the reliability of simulation results when applying dynamic process models to scaled-up applications.
- The works involving transient data generally include the response of the plant to disturbances in a few process variables.
- Most of the validation work was done for flue gas with a typical CO_2 content from coal-based power plants.

Flexible operation of PCC plants has been studied with pilot plant test facilities in test campaigns. Faber et al. [46] conducted open-loop step change responses at the Esbjerg pilot plant; this type of analysis helps in understanding the transient performance of the process. They concluded that the overall system acts as a buffer to perturbations at the plant inlet and that the coupled operation of the absorber/desorber unit led to fluctuations in the system when all parameters—flue gas and solvent mass flow rates and reboiler duty—are changed simultaneously. Bui et al. [47] presented a flexible operation campaign conducted at the Commonwealth Scientific and Industrial Research Organization (CSIRO)'s PCC pilot plant in Australian Gas Light Company (AGL) Loy Yang, a brown-coal-fired power station in Australia. The generated transient data included step changes in flue gas flow rate, solvent flow rate and steam pressure. The purpose of the study was to generate a set of data for validation of dynamic process models, and to gain insight into process behavior under varying operating conditions. A different approach was taken by Tait et al. [48] who conducted experiments that simulated flexible operation scenarios on a pilot plant to treat synthetic flue gas with a CO_2 concentration of 4.3 vol%, typical of a natural gas combined cycle (NGCC) plant. Tests for transient operation have been conducted at the amine plant at CO_2 Technology Center Mongstad (TCM DA). De Koeijer et al. presented two cases: a first case with controlled stop-restart of the plant, driven by a controlled stop of flue gas and steam sent to the PCC plant; and a second case with sudden stop of the blower upstream of the absorber [49]. Nevertheless, a limited amount of transient testing can be conducted during test campaigns. A thoroughly validated dynamic process model can help to study the transient performance, controllability, and flexible operation of the plant and process dynamics via dynamic process simulation.

In this work, a suitable set of steady-state and transient plant data, collected from a MEA campaign at CO_2 Technology Center Mongstad, is selected for dynamic process model validation purposes. The plant was operated with flue gas from a natural gas fueled combined heat and power plant. The selected data is utilized to validate a dynamic process model of the amine-based CO_2 absorption-desorption process at TCM DA. Then, the validated model is employed to carry out two case studies on the process dynamics of the TCM DA amine plant. In the first case study, the open-loop transient response of the pilot plant at different operating loads of the plant is analyzed. In the second case study, the performance of four decentralized control structures of TCM DA amine pilot plant is evaluated for fast disturbances in flue gas volumetric flow rate.

2. Materials and Methods

2.1. Plant Description

CO_2 Technology Center Mongstad test site has a pilot-scale amine-based chemical absorption process plant. The amine plant can be configured to treat flue gas from a catalytic cracker from the Mongstad refinery, with CO_2 content of around 13–14 vol%, typically found in flue gas from coal-fired power plants, and also to treat exhaust gas coming from a combined cycle gas turbine combined heat and power plant (CHP), with CO_2 content of around 3.5 vol%. A fraction of the product CO_2 mass flow rate can be re-circulated back upstream of the direct contact cooler (DCC) to increase the CO_2 content, so CO_2 concentrations of between 3.5 and 13–14 vol% could be fed to the plant to simulate the effects of exhaust gas recirculation [50]. Table 1 presents data of the main process equipment of TCM DA amine plant when configured to treat CHP flue gas, which has a total flue gas capacity of

60,000 Sm^3/h and can capture around 80 ton CO_2/day. Figure 1 shows a simplified process flow sheet of the amine plant at TCM DA when configured for CHP gas. A slipstream of exhaust gas is extracted from the CHP plant placed next to the TCM DA facility, and it consists of about 3% of the total exhaust gas. An induced draft blower is utilized to blow the flue gas flow. It has variable speed drives that allow the flue gas volumetric flow rate fed to the absorber column to be manipulated. Upstream the absorber column, a direct contact cooler cools down and saturates the flue gas with water, by means of a counter-current flow stream of water.

Table 1. Size and materials of main process equipment at the amine plant at TCM DA with CHP stripper configuration.

Absorber	
Column cross sectional area (m^2)	3.55×2
Column height (m)	62
Packing height (12 + 6 + 6) (m)	24
Water wash section height (3 + 3) (m)	6
Absorber packing type	Koch Glitsch Flexipac 2X
Absorber washer packing type	Koch Glitsch Flexipac 2Y HC
CHP Stripper	
Column cross sectional area (m^2)	1.33
Diameter (m)	1.3
Packing height (m)	8
Water wash section height (m)	1.6
Absorber packing type	Koch Glitsch Flexipac 2X
Absorber washer packing type	Koch Glitsch Flexipac 2Y HC
Heat Exchanger L/Rich	
Duty (kW)	10358
Heat transfer area (m^2)	308
Material	SS 316L
Reboiler	
Duty (kW)	3365
Heat transfer area (m^2)	142
Material	SS 316L
Lean Amine Cooler	
Duty (kW)	5182
Heat transfer area (m^2)	78.8
Material	TITANIUM

A chemical absorption process occurs in the absorber column, where the chemical solvent, flowing from top to bottom, meets the flue gas flowing in counter-current. The absorber column consists of a rectangular polypropylene-lined concrete column with a height of 62 m and a cross-section of 2×3.55 m. The absorber-packed sections consisting of Flexipac 2X (Koch-Glitsch Italia, Vimercate, Italy) structured stainless-steel packing are distributed from bottom to top in three sections of 12 m, 6 m and 6 m. Two water-wash systems are installed in the top of the absorption column, consisting of two sections of Flexipac 2Y HC (Koch-Glitsch Italia, Vimercate, Italy) structured stainless-steel packing. The water-wash sections limit emissions and are used to keep the water balance of the plant. The upper water-wash sections can be operated as acid wash [51]. In addition, the plant can be configured to use different packing heights in the absorber column resulting in 12, 18 or 24 m. This can be implemented at TCM plant by introducing all the lean solvent flow at 12 m of absorber packing, 18 m of absorber packing (12 + 6) m or 24 m of absorber packing (12 + 6 + 6) m.
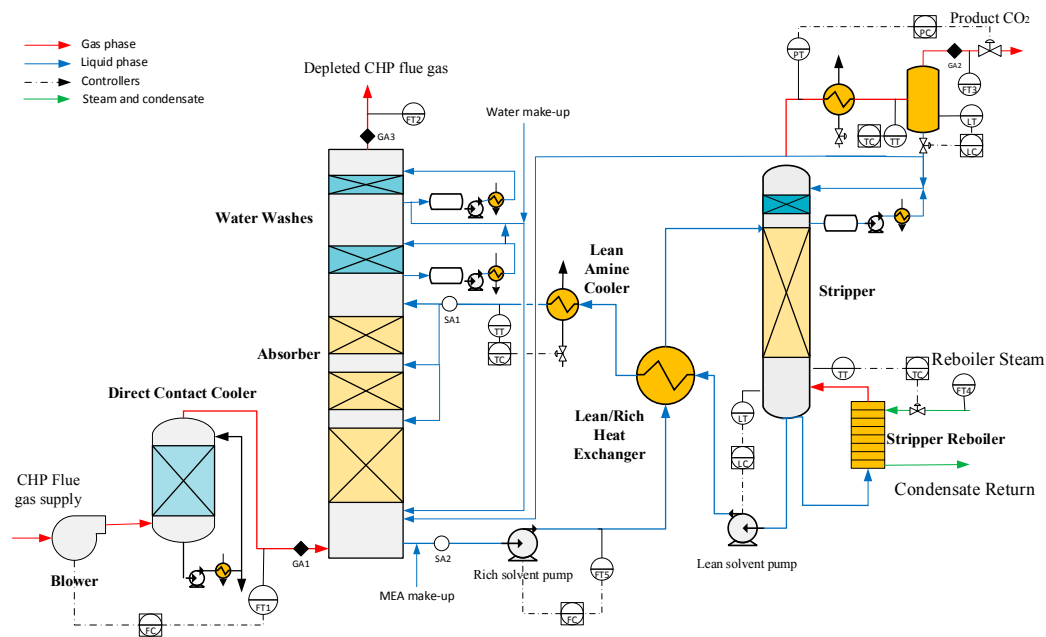
Figure 1. Simplified process flow sheet of the amine plant at CO_2 Technology Center Mongstad, when configured to treat flue gas from a natural gas-fired power plant. The figure shows the location of some gas analyzers (GA), solvent analyzers (SA), flow transmitters (FT), pressure transmitters (PT), temperature transmitters (TT) and level transmitters (LT). The main process controllers of the regulatory control layer are shown, including flow controllers (FC), temperature controllers (TC), pressure controllers (PC) and level controllers (LC).

A 10.4 MW plate and frame heat exchanger is present at the plant where the cold rich amine solution coming from the absorber sump cools down the hot lean amine solution coming from the stripper. In addition, a 5.2 MW lean amine cooler is utilized to set the temperature of the lean solvent conducted to the top of the absorber packing sections, by using a stream of cooling water. The rich solvent is pumped to the top of the stripper column, where it meets the stripping vapors generated in the reboiler. The CHP stripper with overhead condenser system consists of an 8 m column of Koch Glitsch Flexipac 2X structured stainless-steel packing of 1.3-m-diameter, and a water-wash system with Koch Glitsch Flexipac 2Y HC structured stainless-steel packing of 1.6 m of height. The stripper reboiler consists of a 3.4 MW thermosiphon steam-driven system that supplies the heat required for the desorption process. The steam supplied to the reboiler comes from the refinery situated next to the TCM DA facility. Details on the steam supply system can be found in Faramarzi et al. [51].

2.2. Pilot Plant Configuration and Instrumentation

The TCM DA amine plant can be utilized to test various chemical solvents. In this work, the tests were conducted with 30 wt. % aqueous monoethanolamine (MEA). During the tests conducted in the test campaign, the responses and performance of the pilot plant were logged and extracted every 30 s. Gas composition was logged with gas analyzers at the inlet of the absorber, outlet of the absorber, and the product CO_2. A gas chromatograph (GC) installed at TCM DA plant can measure concentrations of CO_2, N_2, H_2O and O_2 at the three locations in a nearly simultaneous manner, which is a desired feature for transient tests; refer to GA1, GA2 and GA3 in Figure 1. Details on gas analyzers and instrumentation at TCM DA plant can be found in [51].

Gas phase flow rates were measured at the plant during the tests. The flue gas volumetric flow rate fed to the absorber is measured with an ultra-sonic flow meter (FT1). As discussed by Faramarzi et al. in [51], the depleted flue gas flow meter (FT2) had a higher degree of variability than FT1, and some transients were observed on the FT2 measurement that were not explained by changes

in process parameters at the plant. Therefore the depleted flue gas flow rate was calculated in the test campaign by considering that all O_2 and N_2 fed to the absorber goes out of the plant with the depleted flue gas. The cooled product CO_2 discharge flow (FT3) was measured with a vortex flow meter. Other flow rates measured at the plant include the steam fed to the reboiler, the lean amine flow rate at the absorber inlet and the rich amine flow rate at the absorber outlet. For flue gas flow meters, the standard conditions are 15 °C and 101.3 kPa [51].

Pressures and pressure drops at different components of the plant were logged. In addition, main process temperatures were logged. For process model validation, it is common to assess the model prediction of the absorber and stripper temperature profiles. Within the absorber and stripper columns of TCM DA's amine plant there are four temperature sensors distributed in the radial plane per meter of packing in the axial direction. Thus, there are 96 temperature sensors within packed segments of absorber column and 28 temperature sensors within the packed segment in the stripper column. These measurements allow the creation of clear temperature profiles of the absorber and stripper columns in the axial direction (at each column height, the resulting temperature value is the average of the four measurements distributed in the radial plane).

Online solvent analysis measurements (SA) were taken at the inlet (SA1) and outlet of the absorber (SA2); refer to Figure 1. The measurements include pH, density and conductivity. In addition, solvent samples were regularly taken manually and analyzed onsite. These analyses allow MEA concentration and CO_2 loadings to be calculated at the sampling points on a periodic basis. The actual reboiler duty was estimated as suggested in Thimsen et al. [52]. Equation (1) shows the calculation of the actual reboiler duty, where F_{steam} is the logged measurement data of steam mass flow rate (refer to FT4 in Figure 1), T_c is the condensate temperature, T_g is the superheated steam inlet temperature, p_g is the steam pressure at inlet, and p_c is the condensate pressure. Enthalpy was calculated with the use of accurate steam tables, with the condensate at the reboiler outlet assumed to be saturated liquid at T_c or p_c. The specific reboiler duty (*SRD*) in kJ/kgCO_2 is calculated as in Equation (2), where F_{prod} is the CO_2 rich product mass flow rate; refer to FT3 in Figure 1.

$$\dot{Q}_{reb} = F_{steam}\left(h_g\left(T_g, p_g\right) - h_c(T_c, p_c)\right) \tag{1}$$

$$SRD = \frac{\dot{Q}_{reb}}{F_{Prod}} \tag{2}$$

During the tests presented in this work, the averaged total inventory of aqueous MEA was around 38.2 m^3. Averaged values of liquid hold-ups and its distribution at different components of the plant during the steady-state tests included in this work are presented in Table 2. Detailed data on solvent inventory distribution throughout the plant is of importance in order to obtain suitable dynamic process simulation results. The regulatory control layer of the plant was active during the tests conducted in the MEA campaign. The main control loops of the regulatory control layer are presented in Figure 1. Note that the actual regulatory control layer of the amine plant at TCM DA is more complex and includes more control loops for auxiliary equipment, stable and safe operation of the plant, and start-up and shut-down sequences. The control loops included here are those the authors found relevant for the purposes of dynamic process modeling and simulation of this plant during online operation, and considering the time scales of interest for process operation.

Table 2. Averaged values of total solvent inventory and its distribution within the main components of the TCM plant.

PCC Plant Main Components	Solvent Inventory (m³)
Absorber sump	8.1
Absorber packing	8.4
CHP stripper packing	1.0
CHP stripper sump	2.3
CHP reboiler	0.4
Cold rich solvent pipe	2.2
Cold lean solvent pipes	5.2
Hot rich solvent pipe	1.1
Hot lean solvent pipes (including reboiler pipes)	8.2
Lean/rich hx—lean side	0.5
Lean/rich hx—rich side	0.5
Lean cooler	0.3
TOTAL	38.2

2.3. Dynamic Process Model

Dynamic process modeling was carried out by means of the physical modeling language Modelica [53]. Modelica allows development of systems of differential and algebraic equations that represent the physical phenomena occurring in the different components of the system. The process models of the equipment typically found in a chemical absorption plant were obtained from a Modelica library called Gas Liquid Contactors (Modelon AB, Lund, Sweden) [54], and the commercial tool Dymola (Dassault Systèmes, Vélizy-Villacoublay, France) [55] was utilized to develop the models and carry out the simulations. The component models include absorber and stripper columns, sumps, lean and rich heat exchanger, stripper reboiler, overhead condenser, condensers, pipe models, pumps, valves, measurements and controllers. The dynamic process model of the amine plant at TCM DA presented in Figure 1 was developed by parameterizing, modifying and connecting the different models. For this purpose, the main process equipment, size, geometry and materials were considered; refer to Table 1. A key aspect for obtaining suitable dynamic simulation results is the consideration of the distribution of solvent inventory at the different equipment of the plant. Therefore, solvent inventory distribution was implemented in the dynamic process model; refer to Table 2. Finally, the equivalent regulatory control layer of the plant was applied in the dynamic process model; discussed later in Section 5.2. The models contained in the library have been presented elsewhere [56,57]; therefore only an overview of the models is presented in the following. Numerical integration of the resulting system of differential and algebraic equations was carried out in Dymola with the differential algebraic system solver (DASSL) implemented in Dymola [55]. The main assumptions applied are [56]:

- All chemical reactions occur in the liquid phase and are assumed to be in equilibrium.
- The flue gas into the absorber contains only CO_2, O_2, H_2O and N_2.
- MEA is non-volatile and not present in the gas phase.
- The total amount of liquid in the column is defined as the packing hold-up and the sump liquid hold-up.
- The reboiler is modeled as an equilibrium flash stage.
- The liquid in the column sumps and other large volumes are assumed to be ideally mixed.
- Mass and heat transfer between liquid and gas phase is restricted to packed section.
- Negligible temperature difference between the liquid bulk and interface to gas phase.
- No storage of mass and energy in the gas phase.
- All liquid from the packing bottom in the stripper is fed to the reboiler with a constant liquid level.
- Constant target packing hold-up.

The models of the absorber and stripper columns are developed based on the two-film theory; therefore, at the gas and liquid interface thermodynamic equilibrium is assumed. Interface mass transfer phenomena is modeled in packed sections with a rate-based approach with enhancement factor E [30], which takes into account the enhanced mass transfer due to chemical reactions; refer to Equations (3) and (4), where $c_{i,if}$ and $c_{i,b}$ are molar concentrations at liquid bulk and interface, A_{if} is the contact area, k_i are the mass transfer coefficients by Onda [58], T is the bulk phase temperature, and p_i are the partial pressures of the species in the gas phase. The pseudo-first order enhancement factor E is calculated as in Equation (5), where k_{CO_2} is the overall reaction constant for CO_2 and C_{MEA} the molar free MEA-concentration taken from [59], the diffusivity D_{CO_2} of CO_2 in aqueous MEA is calculated by the Stokes-Einstein relation and the diffusivity of CO_2 in water from [60]. C_{ef} is a pre-multiplying coefficient for calibration of enhancement factor. The packing characteristics of Koch Glitsch Flexipac 2X were considered for parameterizing the packing segments of the dynamic process model for absorber and stripper columns, with a surface area of 225 m^2/m^3 and a void fraction of 0.97.

$$\dot{n}_{i,l} = A_{if} k_{i,l} E \left(c_{i,b} - c_{i,if} \right) \qquad i = CO_2 \tag{3}$$

$$\dot{n}_{i,v} = \frac{A_{if} K_{i,v} \left(p_{i,b} - p_{i,if} \right)}{RT} \qquad i = CO_2, \ H_2O \tag{4}$$

$$E = C_{ef} \frac{\sqrt{C_{MEA} k_{CO_2} D_{CO_2}}}{k_{i,l}} \qquad i = CO_2 \tag{5}$$

Phase equilibrium at the gas-liquid interface is calculated as in Equations (6) and (7), where the solubility of CO_2 in water is considered by Henry's law, with He_i from [61]; activity coefficients γ_i are implemented from [61]; chemical equilibrium is assumed at the interface and liquid bulk, and the chemical equilibrium constants K_i implemented in the process model are obtained from Böttinger [61]. The Van't Hoff equation is utilized in order to infer the heats of reaction ΔH_r from the equilibrium constant; refer to Equation (8). The Chilton-Colburn analogy was employed to correlate sensible heat transfer between phases with the gas phase mass transfer coefficient. Latent heat connected to the transferred mass flow from one phase to the other is considered in the specific enthalpies of the individual species. The heat of evaporation and heat of solution are a function of temperature but are considered constant with solvent CO_2 loading. The gas phase model assumes ideal gas law, and the pressure of the column p is determined by the gas phase pressure drop.

$$y_i p = \gamma_i x_i \ He_i \ i = CO_2 \tag{6}$$

$$y_i p = \gamma_i x_i \ p_{i,sat}(T) \ i = H_2O \tag{7}$$

$$\frac{dlnK}{dT} = \frac{\Delta H_r}{RT^2} \tag{8}$$

The lean-rich heat exchanger is modeled as a static heat exchanger model with the ε-NTU (effectiveness—number of thermal units), and pure transport delay models are used to account for dead times included by the solvent hold-up within piping' volumes.

At the top of the absorber column a washer model is implemented, consisting of a volume model with phase separation that saturates the gas with water at the targeted temperature. A make-up stream of water is injected in the absorber sump to keep the H_2O mass balance of the system. MEA is assumed non-volatile in the model and therefore it is only present in the liquid phase. However, in the actual plant make-up MEA is required for operation and it is injected upstream the rich amine pump; refer to Figure 1.

3. Steady-State Validation of Dynamic Process Model

3.1. Steady-State Operating Cases

A test campaign was conducted at the amine plant at TCM DA using MEA, operated from 6 July until 17 October 2015. Table 3 shows the steady-state cases generated during the test campaign that were used in this work for dynamic process model validation purposes. The plant was operated with 30 wt. % MEA for all cases. The objective was to select a set of steady-state cases from the MEA campaign that could represent a wide range of steady-state operating conditions, including data from full capacity of volumetric flow rate fed to the absorber column. The steady-state cases were generated by varying the set points of the main pilot plant inputs, namely solvent circulation flow rate F_{solv} (refer to FT5 in Figure 1), reboiler duty ($\dot{Q}_{reb}$), and flue gas volumetric flow rate (F_{gas}). The steady-state cases represent a variation in operating conditions of the plant, especially on the flue gas volumetric flow rate load of the absorber, CO_2 capture rate, L/G ratio in the absorber and absorber packing height. Cases 1 to 5 are operated at absorber full flue gas capacity of around 60,000 Sm^3/h. A similar mass-based L/G ratio, of around 0.89, is kept in the absorber column during the steady-state operating cases with full capacity, with the exception of Case 4, where it is changed to 0.8, by varying the rich solvent mass flow rate. The main process variability in these cases is the change in reboiler duty, with CO_2 capture rate ranging from 85 to 68%. CO_2 capture rate was calculated with the method 1 described by Thimsen et al. [52]; refer to Equation (9), where F_{prod} refers to the product CO_2 flow rate (FT3 in Figure 1), and X_{CO_2} is the mass fraction of CO_2 in the absorber inlet (measured at GA1 in Figure 1). Note that here CO_2 capture rate has been named *Des* as it defines the desorption ratio utilized in Section 5.2. In addition, Cases 2 to 5 were operated with 18 m absorber packing, i.e., the uppermost absorber-packing segment is kept dry. Cases 6 to 10 are operated with 24 m absorber packing and the absorber column at 80% volumetric flue gas flow rate capacity. The mass-based L/G ratios on the absorber range from 1.34 to 0.75 for Cases 6 to 10, by varying solvent circulation mass flow rate. The capture rate is kept constant at around 85% by varying the reboiler duty.

Table 3. A selection of steady-state data cases obtained from the test campaign conducted at TCM plant during autumn 2015. The plant was operated with 30 wt. % aqueous MEA.

Case	1	2	3	4	5	6	7	8	9	10
Gas flow rate (Sm^3/h)	59,461	59,468	59,442	59,499	59,544	46,973	46,973	46,973	46,973	46,973
Rich solvent flow rate (kg/s)	17.33	17.31	17.22	15.50	17.24	20.56	17.50	16.11	12.74	11.46
L/G ratio (kg/kg)	0.89	0.89	0.89	0.80	0.89	1.34	1.14	1.05	0.83	0.75
Reboiler duty (kW)	3417	3159	2664	2397	3056	2745	2669	2667	2659	2682
Absorber inlet gas CO_2 (vol%)	3.64	3.61	3.59	3.58	3.59	3.60	3.62	3.62	3.62	3.62
Absorber inlet gas O_2 (vol%)	15.52	15.54	15.55	15.46	15.35	15.30	15.48	15.49	15.51	15.52
Absorber inlet gas H_2O (vol%)	3.98	3.92	3.93	4.01	4.22	3.80	3.36	3.46	3.52	3.43
Absorber inlet gas N_2 (vol%)	79.09	79.02	78.85	78.57	78.20	78.18	78.88	78.94	79.06	78.96
Loading rich (mol/mol)	0.490	0.485	0.498	0.500	0.495	0.475	0.488	0.486	0.493	0.491
Loading lean (mol/mol)	0.280	0.294	0.333	0.341	0.314	0.342	0.329	0.310	0.260	0.229
Stripper bottom temperature (°C)	120.9	121.1	119.3	118.9	120.1	116.6	118.3	119.1	121.4	121.8
CO_2 product flow (kg/s)	0.95	0.89	0.75	0.68	0.84	0.74	0.74	0.75	0.77	0.76
CO_2 capture rate (%)	85	80	68	-	75	85	85	85	85	85
Absorber packing height (m)	24	18	18	18	18	24	24	24	24	24

The first series of tests during the MEA campaign were dedicated to verification of mass balances of the plant [50]. CO_2 mass balance gives results close to 100%, and Gjernes et al. [50] conclude that CO_2 mass balance based on gas phase can be maintained at a level better than $100 \pm 5\%$. In this work, the suggested method in [50] was used during data selection in order to ensure that the steady-state data cases presented in Table 3 have acceptable CO_2 mass balance.

In order to develop the overall dynamic process model of the plant, the steady-state data for Case 1, refer to Table 3, was used as a reference to calibrate the dynamic process model, and the main outputs from the model simulations were compared with the plant data. This data set was chosen since

it represents the baseline operating conditions of the amine plant at TCM DA when using aqueous MEA as chemical solvent, as presented in Faramarzi et al. [51]. The models of the different subsystems of the plant consisting of (i) absorber column; (ii) lean/rich heat exchanger; and (iii) stripper column with overhead condenser and reboiler were calibrated separately, and then linked to form the overall dynamic process model. The model was calibrated by tuning a pre-multiplying coefficient C_{ef} for the enhancement factor E. It was set to 0.28 in absorber packed segments and 0.01 in stripper packed segments. The validation section included in this work extends on work conducted previously [62].

$$Des = \frac{F_{prod}}{F_{gas} \cdot X_{CO_2}} \tag{9}$$

3.2. Validation Results of Dynamic Process Model with Steady-State Plant Data

The results from the simulated dynamic process model for the steady-state operating cases, described in Section 3.1, are displayed in Table 4. The results shown are for main process variables during pilot plant operation, namely CO_2 lean (L_l) and rich (L_r) loadings, product CO_2 flow rate (F_{prod}), specific reboiler duty (SRD) and stripper bottom temperature T_{str}. Possible deviations in dynamic process model prediction arise from errors related to measurement uncertainty and to modeling uncertainty, the latter being related to the fact that a physical model is always a simplification of reality. This means that it is natural to observe some deviation in the prediction of the dynamic process model simulation. Therefore, it is of importance to quantify these errors so that they are kept within reasonable bounds. The absolute percentage errors (AP) and the mean absolute percentage errors (MAP) are calculated as in Equations (10) and (11), where x_m is the value of the process variable predicted by the process model simulation, x_p is the value of the process variable measured at the pilot plant at the given steady-state operation case, and n is the number of steady-state cases studied.

$$AP = 100 \cdot \left| \frac{(x_m - x_p)}{x_p} \right| \tag{10}$$

$$MAP = 100 \cdot \sum_i^n \frac{\left| \frac{(x_{m,i} - x_{p,i})}{x_{p,i}} \right|}{n} \tag{11}$$

The results for lean CO_2 loading are presented in Figure 2 with a parity plot, where $\pm 5\%$ and $\pm 10\%$ error lines are also shown. It is clear that the dynamic process model under-predicts lean loading for most of the cases, with a $MAP < 6.6\%$. In addition, Figure 2 shows the parity plot for CO_2 product flow rate; in this case, the CO_2 product flow rate is also under-predicted by the dynamic process model, with a $MAP < 5.3\%$. Figure 3 shows the parity plot for stripper bottom temperature, with the $\pm 2\%$ error lines plotted; stripper bottom temperature T_{str} presented a $MAP < 1\%$. From the parity plots, one can observe that, despite the errors found in the absolute values predicted by the dynamic process model with respect to the reference plant data, the dynamic process model can predict the variability in the main process variables for a wide range of steady-state operating conditions.
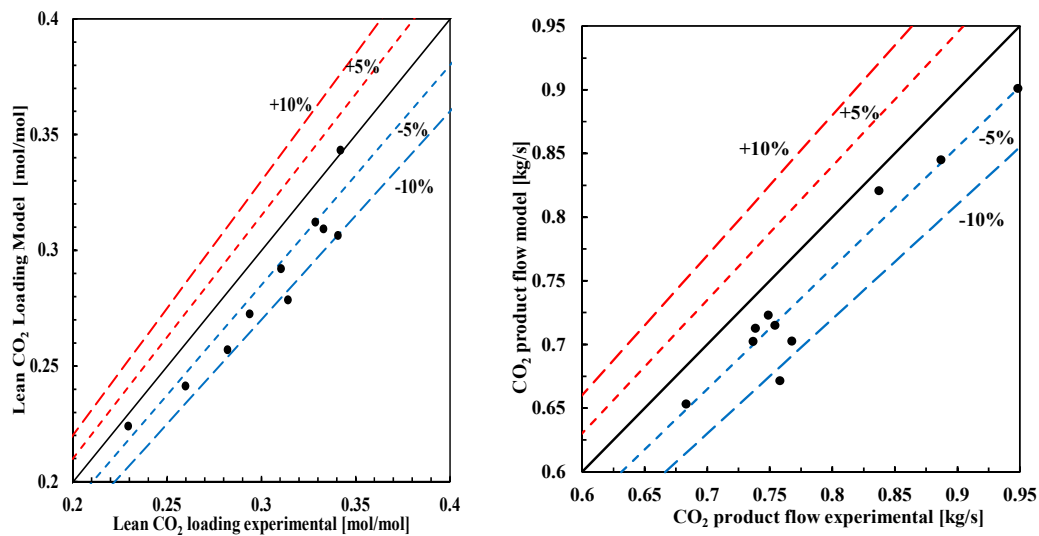
Table 4. Results from dynamic process simulation of the amine plant at TCM for the 10 steady-state operation cases. The pilot plant data for solvent CO_2 lean loading (L_l), solvent CO_2 rich loading (L_r), CO_2 product flow rate (F_{prod}), specific reboiler duty (SRD) and stripper bottom temperature (T_{str}) are shown. In addition, the model prediction during steady-state simulation for the same process variables is shown. Calculated absolute percentage errors (AP) and mean absolute percentage errors (MAP) between pilot plant measurements and simulated model predictions for the 10 steady-state operating cases are presented.

Case		1	2	3	4	5	6	7	8	9	10
Rich loading L_r (mol/mol)	Pilot plant	0.489	0.485	0.498	0.500	0.495	0.475	0.488	0.486	0.493	0.491
	Model	0.514	0.513	0.514	0.514	0.513	0.512	0.513	0.514	0.514	0.514
	AP	5.01	5.58	3.19	2.91	3.55	7.81	5.17	5.62	4.43	4.70
	MAP										4.80
Lean loading L_l (mol/mol)	Pilot plant	0.282	0.294	0.333	0.341	0.314	0.342	0.329	0.310	0.260	0.229
	Model	0.257	0.273	0.309	0.306	0.279	0.343	0.312	0.292	0.241	0.224
	AP	8.93	7.24	7.16	10.06	11.34	0.35	4.98	5.94	7.10	2.35
	MAP										6.55
CO_2 Product flow F_{prod} (kg/sec)	Pilot plant	0.95	0.89	0.75	0.68	0.84	0.74	0.74	0.75	0.77	0.76
	Model	0.90	0.84	0.72	0.65	0.82	0.70	0.71	0.72	0.70	0.67
	AP	4.97	4.72	5.18	4.38	1.96	4.65	3.50	3.44	8.46	11.42
	MAP										5.27
Specific reboiler duty SRD (kJ/kg)	Pilot plant	3602	3562	3533	3509	3651	3727	3613	3561	3463	3538
	Model	3791	3739	3726	3670	3724	3909	3744	3688	3783	3994
	AP	5.23	4.95	5.46	4.58	2.00	4.88	3.63	3.56	9.24	12.89
	MAP										5.64
Stripper bottom temperature T_{str} (°C)	Pilot plant	120.9	121.1	119.1	118.9	120.1	116.6	118.3	119.1	121.4	121.8
	Model	121.0	119.8	117.2	117.2	119.4	114.7	117.0	118.3	121.0	121.8
	AP	0.08	1.06	1.63	1.42	0.61	1.62	1.10	0.71	0.31	0.04
	MAP										0.86

Figure 2. Parity plots of lean CO_2 loading (**left**) and CO_2 product flow rate (**right**). Lines for +10%, +5%, −5% and −10% percentage error are shown. The mean percentage error is <6.6% for CO_2 lean loading and <5.3% for product CO_2 flow rate (F_{prod}).
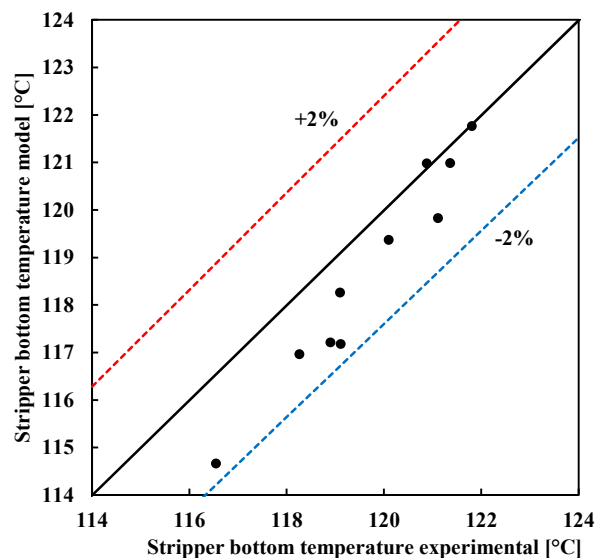

Figure 3. Parity plot for stripper bottom temperature for the 10 steady-state operation cases. Lines for +2% and −2% percentage errors are shown. The mean percentage error is 0.86 for stripper bottom temperature.

Temperature within absorber and stripper column is an important process variable since it affects phase equilibrium at liquid and gas-liquid interface. Some important model parameters and thermophysical properties depend on temperature, including heat capacity, water heat of condensation, heats of reaction, equilibrium constants and CO_2 solubility. Therefore, it is desirable that the dynamic process model can predict with good accuracy absorber and stripper columns' temperature profiles. Figure 4 shows the comparison between the pilot plant temperature profiles of the absorber and desorber columns with the predictions from the simulation of the dynamic process models. Two steady-state operating cases are presented: Case 1 (Table 3) with absorber flue gas volumetric capacity of 100%, mass-based L/G ratio of 0.89 and capture target of 85%; and Case 6 (refer to Table 3) with 80% flue gas volumetric capacity, mass-based L/G ratio of 1.34 and capture target of 85%.

Both cases were operated with 24 m of wet absorber packing, and represent two operating cases with different flue gas capacities and L/G ratios.
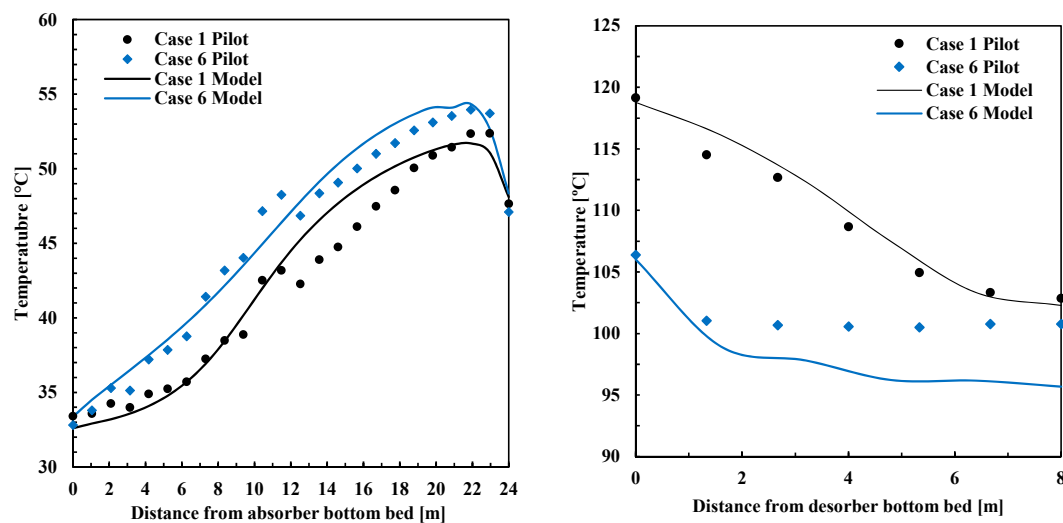
Figure 4. Temperature profiles for absorber column (**left**) and stripper column (**right**) for steady-state cases 1 and 6. In both steady-state operation cases, 24 m of absorber packing were utilized.

Validation of absorber and stripper temperature profiles is normally considered a challenging task for several reasons. At TCM DA the temperature profiles are the resulting averaged values of the 4 measurements distributed radially in a given axial position within the column; refer to Section 3. A given pilot plant temperature value presented in Figure 4 is the resulting average over time during one hour of steady-state operating conditions, of the averaged 4 temperature measurements radially distributed within the absorber or stripper column, at the given axial position of the column. The individual temperature measurements are considered reliable and the resulting temperature profiles are reasonable. However, some sensors are located closer to the center of the packing while others closer to the wall. This results in a maximum variation (<6 °C) which is observed between the measurements in the same radial plane, which depends on operating conditions and is different at different radial planes. Based on the results presented in Figure 4, the dynamic process model can properly predict absorber and stripper column temperature profiles with sufficient accuracy considering the purpose of application. Absorber temperature profiles predicted by the model show a good agreement with the experimental pilot plant data, and the model is capable of properly predicting the trends in temperature along the column. The absorber temperature profiles have a mean absolute percentage error (<2.5%) for Case 1 and (<2.1%) for Case 6, which is within the observed maximum variability of the temperature measurements in a given radial plane. In addition, desorber temperature profiles have a mean average error (<0.6%) for Case 1 and (<3.6%) for Case 6. It is the desorber temperature profile for Case 6 that presents the less accurate prediction. In addition, it can be concluded that the process model is capable of properly predicting the variation of temperature profiles for various steady-state operating conditions.

4. Validation of Dynamic Process Model with Transient Plant Data

For dynamic process model validation purposes transient tests are conducted by means of open-loop step changes in the main process inputs to the plant. The transient behavior occurs between the initial steady-state operating conditions until the new steady-state operating conditions are reached. In this work, the experiments consist of set-point changes in rich solvent flow rate, flue gas volumetric flow rate fed to the absorber and reboiler duty. The output trajectories of main process variables are observed and compared with the model output trajectories. In order to obtain good sets of data

for validation, it is desired to apply the step changes in plant inputs in a non-simultaneous manner. However, this is not normally easy to implement in practice. In order to compare the pilot plant experimental output trajectories with the output trajectories predicted by the dynamic process models, input trajectories were utilized in the dynamic simulations. This means that the measured time series of the inputs applied to the pilot plant during the tests were applied as disturbances or inputs to the dynamic process model; refer to Figures 5a, 6a and 7a. During the three tests, the regulatory control layer of the plant was active. In Figures 5 and 6, the time $t = 0$ corresponds to the point from which the set point of flue gas volumetric flow rate was changed. In Figure 7 the time $t = 0$ is the point from when the set point of rich solvent flow rate was changed.

(a)

(b)

(c)
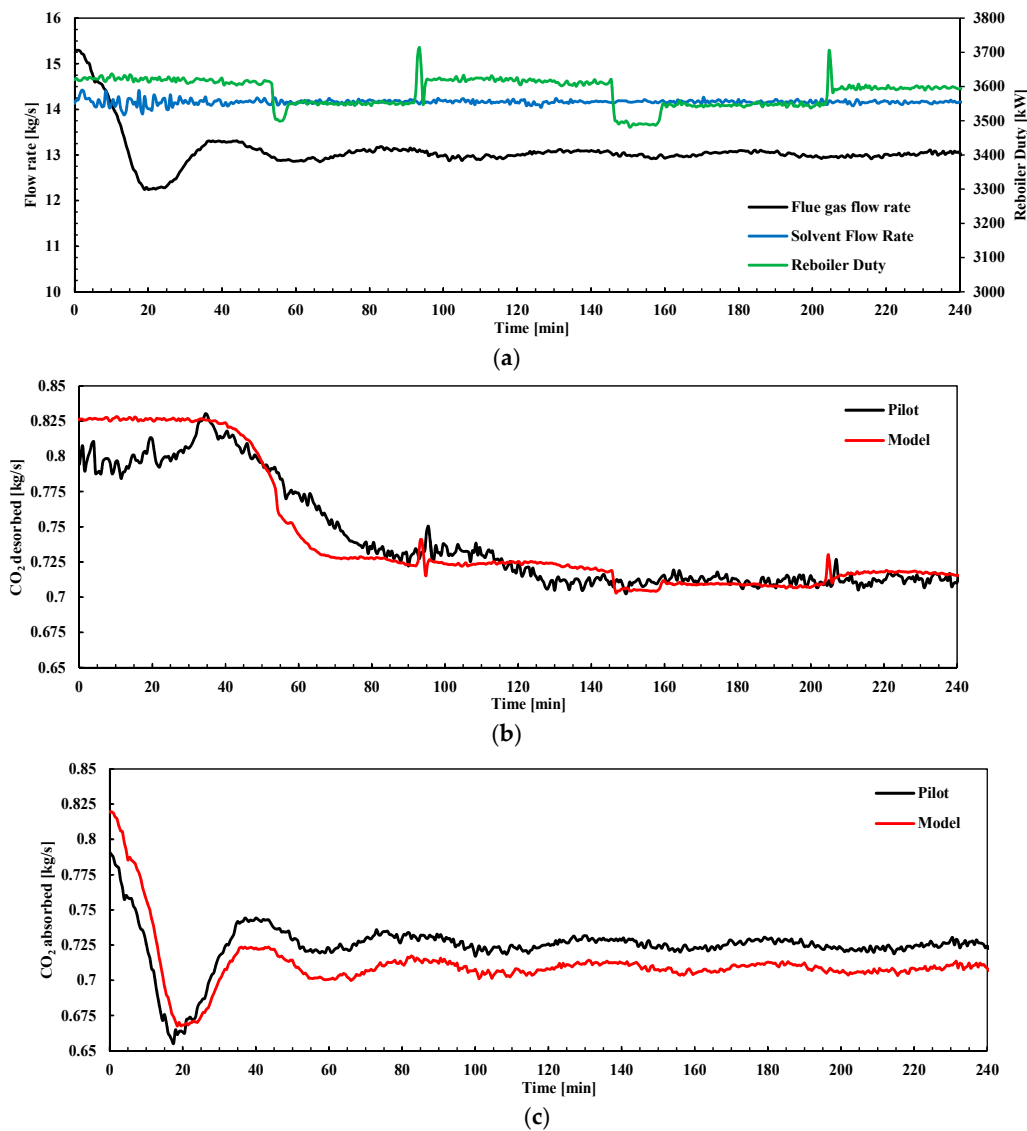
Figure 5. (**a**) Main inputs to the plant for test with flue gas flow rate set-point reduction (kg/s). Rich solvent flow rate from absorber (kg/s) and reboiler duty (kW); (**b**) Pilot plant transient response and model output trajectory for CO_2 product flow rate F_{prod} or CO_2 desorbed (refer to FT3 in Figure 1); (**c**) Pilot plant transient response and model output trajectory for CO_2 absorbed in absorber column, refer to Equation (11). The time $t = 0$ corresponds to the point from which the set point of flue gas volumetric flow rate was changed.
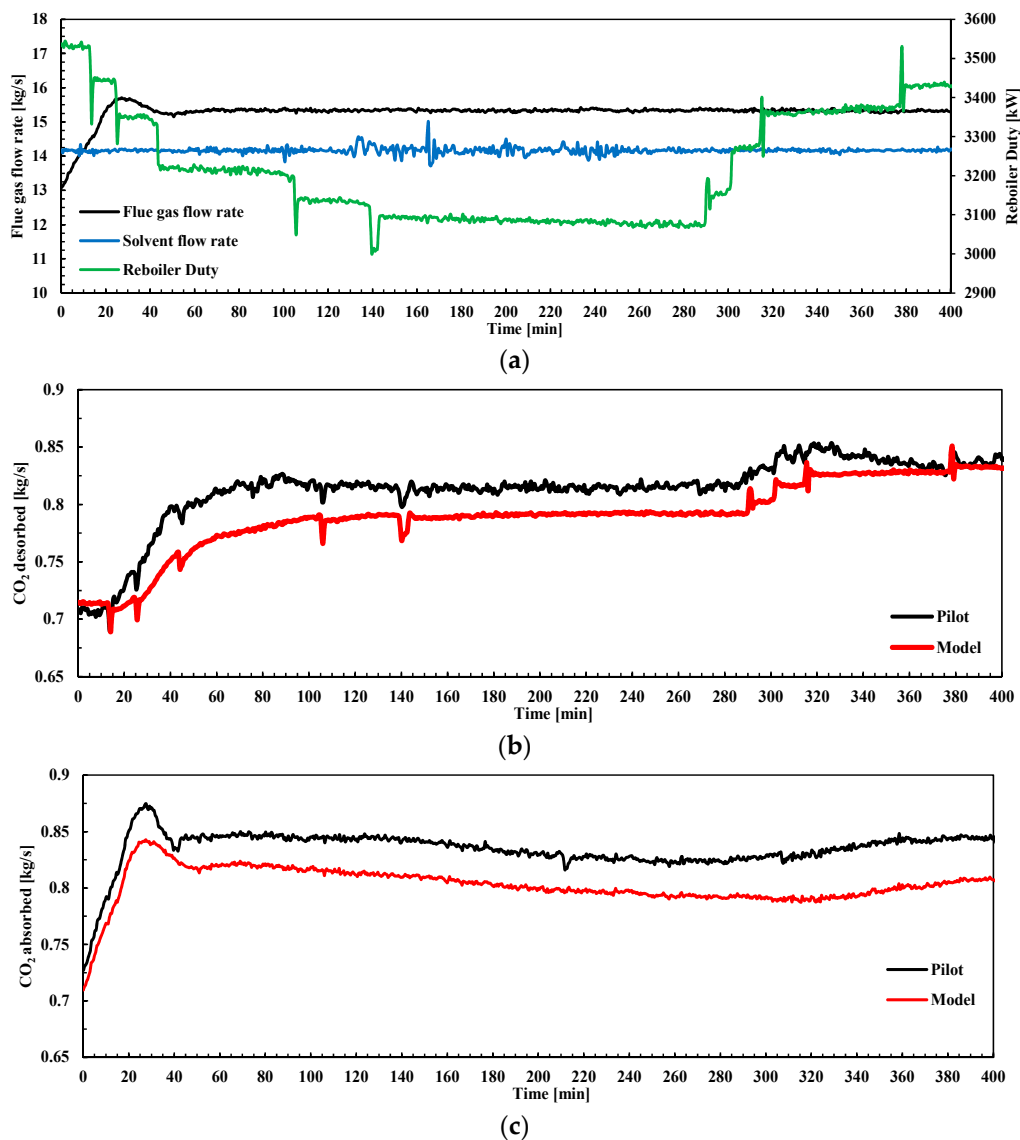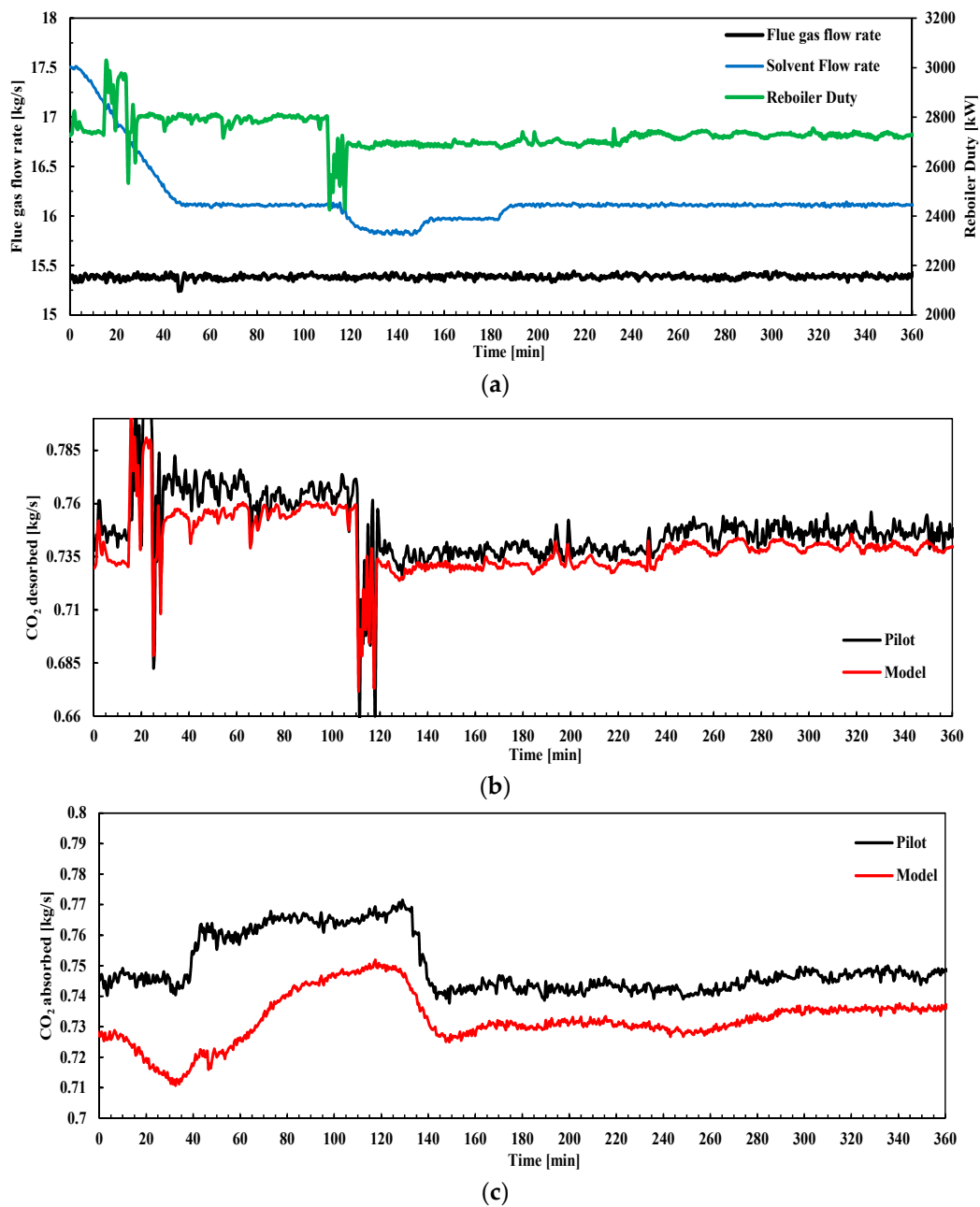
(a)

(b)

(c)

Figure 6. (**a**) Main inputs to the plant for test with flue gas flow rate set-point increase (kg/s). Rich solvent flow rate from absorber (kg/s) and reboiler duty (kW); (**b**) Pilot plant transient response and model output trajectory for CO_2 product flow rate F_{prod} or CO_2 desorbed (refer to FT3 in Figure 1); (**c**) Pilot plant transient response and model output trajectory for CO_2 absorbed in absorber column, refer to Equation (11). The time $t = 0$ corresponds to the point from which the set point of flue gas volumetric flow rate was changed.

(a)

(b)

(c)

Figure 7. (**a**) Main inputs to the plant. Flue gas volumetric flow rate set-point change increase (kg/s). Rich solvent flow rate from absorber (kg/s) and steam flow to reboiler (kg/s); (**b**) Pilot plant transient response and model output trajectory for CO_2 product flow rate F_{prod} or CO_2 desorbed (refer to FT3 in Figure 1); (**c**) Pilot plant response in CO_2 absorbed mass flow rate (kg/s). The time $t = 0$ corresponds to the point from which the set point of rich solvent flow rate was changed.

4.1. Flue Gas Flow Rate Ramp-Down

The main disturbance applied in this transient test consisted of a reduction in flue gas volumetric flow rate at the inlet of the absorber. It was implemented at TCM DA pilot plant by changing the set point of the blower cascade controller from 47,000 Sm^3 to 40,000 Sm^3; refer to FT1 in Figure 1. This corresponds with flue gas volumetric flow capacities in the absorber column of 80% and 67% respectively. Figure 5a shows the three main inputs of the plant for this test. During the test, reboiler duty was changed in steps around the value of 3550 kW; this might be due to the effects of the

regulatory control layer on steam mass flow rate. The solvent mass flow rate had small amplitude oscillations around the set point.

$$CO_{2,abs} = F_{gas} \cdot X_{CO_2} - F_{depleted} \cdot X_{CO_2,out} \qquad (12)$$

Figure 5b,c show the output trajectories of CO_2 product flow rate (or CO_2 desorbed) and CO_2 absorbed to the disturbance applied in this test. CO_2 absorbed is calculated as the difference between CO_2 mass flow rate at the absorber inlet and the CO_2 mass flow rate leaving the absorber with the depleted flue gas at the top of the absorber; refer to Equation (12). In Figure 5b, a dead time of around 40 min was observed, i.e., no significant changes are found in the CO_2 desorbed until around 40 min after the disturbance was applied to the pilot plant. In addition, the plant did not reach steady-state operating conditions until around 4 h later. As shown in Figure 5c, there is not significant dead time in the response of CO_2 absorbed. The difference observed between the output trajectories is characteristic of the coupled transient performance of the absorber and stripper columns. Figure 5b,c shows that the process model is capable of predicting the main process dynamics for CO_2 product mass flow rate (CO_2 desorbed), including an adequate prediction of dead times and stabilization time. In addition, the CO_2 absorbed transient performance trends are predicted in a satisfactory manner.

4.2. Flue Gas Flow Rate Ramp-Up and Step Changes in Reboiler Duty

These tests consist of combined input changes to the plant in terms of flue gas volumetric flow rate and reboiler duty. A set-point increase of the flue gas volumetric flow rate fed to the absorber from 40,000 to 47,000 Sm^3/h was applied. This corresponds with 67% and 80% of the absorber column capacity, respectively. In addition, step-changes in reboiler duty were applied during the transient test. Figure 6a shows the three main inputs of the plant during the test. Figure 6b,c show the CO_2 product flow and CO_2 absorbed for the model and the pilot plant data. In this test a dead time of around 20 min in the response of CO_2 desorbed was observed. This confirms the buffering effect by the chemical process in terms of the response of CO_2 desorbed when the flue gas volumetric flow rate is changed. There is evidence to support this observation in previous pilot plant studies [46–48]. The delay in the response is partly attributed to solvent circulation time and the redistribution of liquid. Despite the steady-state offset shown on CO_2 absorbed in Figure 6b, a good prediction of the main transient response is seen. It is possible that the reduction in reboiler duty at around 10 min flattens out the response in CO_2 product flow rate.

4.3. Solvent Flow Rate Ramp-Down

In this test, the plant is operated in steady-state until the rich solvent mass flow rate set point is ramped down from around 17.5 kg/s to around 16.1 kg/s; refer to FT5 in Figure 1. The reboiler duty and flue gas volumetric flow rate were intended to be kept constant. Figure 7a shows the three main inputs of the plant during this transient test. In addition, the pilot plant performance in terms of product CO_2 mass flow F_{prod} (or CO_2 desorbed) and absorbed CO_2 flow rate are presented, together with the dynamic process model simulations for this test. Again, a satisfactory agreement is found between the plant trajectories and the output trajectories predicted by the dynamic process model.

From the three transient tests presented above, it can be concluded that the dynamic process model predicts the transient trends of the main output trajectories of the process for different inputs to the plant. In addition, the dead times and stabilization times of the process are properly predicted by the dynamic process models, despite the steady-state deviations observed and already quantified in Section 3.2. This means that the dynamic process model is suitable for simulation studies at the plant scale, including dynamic process simulations to analyze the plant transient performance, and for control tuning and advanced control layer design, including control structure studies.

5. Case Study: Open-Loop Performance and Decentralized Control Structures

5.1. Open-Loop Step Responses at Different Plant Flue Gas Capacities

A power plant operated in a power market with a high penetration of renewables will most likely be operated in load-following mode [7,63]. This means that the power plant with PCC will be operated during a significant amount of its lifetime at part loads. In the case of a natural gas combined cycle power plant with post-combustion CO_2 capture it means that, at part-load operation, the gas turbine (GT) load will be reduced, generating a reduced mass flow rate of flue gas that would be conducted to the PCC unit. The purpose of this case study is to investigate the transient performance of the PCC pilot plant via dynamic process simulation by implementing open-loop step changes to the dynamic process model, and to compare the response of the plant at different part-load operating points, defined by different mass flow rates of flue gas to be treated. The analysis will assess the transient response of the plant to multiple and non-simultaneous step changes in three key inputs to the plant, namely (i) flue gas flow rate F_{gas} (ii) solvent flow rate F_{solv}; and (iii) reboiler duty $\dot{Q}_{reb}$, at different flue gas mass flow rate capacities of the plant. In order to define the part-load operating points, a decentralized control structure was utilized, in which reboiler duty was the manipulated variable to control stripper bottom temperature T_{str} to 120.9 °C, and the solvent flow rate was the manipulated variable to control CO_2 capture ratio *Cap* to 0.85, as defined in Equation (13). When operating the plant at different flue gas mass flow rates, corresponding to 100%, 80% and 60% of nominal mass flow rate, this results in the three steady-state operating points presented in Tables 5 and 6. The control structure is defined as control structure A in Table 7.

$$Cap = \frac{F_{gas} \cdot X_{CO_2} - F_{depleted} \cdot X_{CO_2,out}}{F_{gas} \cdot X_{CO_2}} \tag{13}$$

Table 5. Simulated pilot plant inputs' set points for the three operating points to be studied, corresponding to 100%, 80% and 60% of flue gas mass flow rate capacity of the pilot plant. With *Cap* = 0.85 and T_{str} = 120.9 °C for all cases.

Pilot Load (%)	F_{gas} (kg/h)	F_{solv} (kg/s)	$\dot{Q}_{reb}$ (MW)
100	19.3	17.6	3.5
80	15.3	13.2	2.7
60	11.6	9.5	2.1

Table 6. Simulated pilot plant values for the process variables, lean CO_2 loading L_l, rich CO_2 loading L_r, CO_2 capture ratio *Cap* and CO_2 product flow rate, at three different operating points of the plant, corresponding to 100%, 80% and 60% of flue gas mass flow rate capacity of the pilot plant. With *Cap* = 0.85 and T_{str} = 120.9 °C for all cases.

Pilot Load (%)	L_l (mol/mol)	L_r (mol/mol)	*Cap*	F_{prod} (kg/s)
100	0.280	0.501	0.85	0.91
80	0.246	0.514	0.85	0.72
60	0.228	0.514	0.85	0.55

Table 7. Control structures for the supervisory control layer of the TCM amine plant. Key manipulated variables (MVs) are solvent flow rate F_{solv} and reboiler duty Q_{reb}. Controlled variables are CO_2 capture ratio *Cap* to 85%, defined in Equation (12), and stripper bottom temperature T_{str} to 120.9 °C. Control structure D controls *Cap* via a feed forward FF controller.

Control Structure	Pairing 1		Pairing 2	
	Manipulated Variable	**Controlled Variable**	**Manipulated Variable**	**Controlled Variable**
A	F_{solv}	*Cap*	Q_{reb}	T_{str}
B	Q_{reb}	*Cap*	F_{solv}	T_{str}
C	F_{solv}	*L/G*	Q_{reb}	T_{str}
D	F_{solv}	*Cap, with FF*	Q_{reb}	T_{str}

The open-loop response was studied for the process variables (i) CO_2 absorbed $CO_{2,abs}$, in Equation (11); (ii) CO_2 desorbed $CO_{2,abs}$ (or F_{prod}); (iii) lean CO_2 loading L_l at the inlet of the absorber; and (iv) rich CO_2 loading L_r at the outlet of the absorber. To characterize the transient response, dead time θ, settling time t_s, total stabilization time t_t, and relative change (*RC*) were calculated:

- Dead time θ: it is the time that takes before a process variable starts to change from the initial steady-state conditions as a response to the disturbance or input.
- Settling time: The 10% settling time t_s is the time taken from when the process variable begins to respond to the input change (dead time) until it remains within an error band described by 10% of the change in the process variable Δy and the final steady-state value of the process variable y_∞, i.e.: $-0.1\,\Delta y + y_\infty < y_\infty < 0.1\,\Delta y + y_\infty$.
- Total stabilization time: the sum of the dead time θ and the settling time t_s is the resulting total stabilization time t_t.
- Relative change *RC:* Change in the observed process variable from initial steady-state conditions y_0 to the final steady-state conditions; refer to Equation (14).

$$RC(\%) = 100 \cdot \frac{y_\infty - y_0}{y_0} \tag{14}$$

The detailed results of the process simulations are presented in Tables A1–A3 in Appendix A. Figure 8 shows the total stabilization times for the selected process variables at the three operating points, for step changes in solvent flow rate and reboiler duty. The responses for step changes in flue gas flow rate are not presented, since it is shown in Table A1 that the relative change *RC* in the output process variables is very small or negligible (*RC* ranges from −0.81% to 0.21%). This can be explained by the highly diluted nature of the CO_2 in the flue gas (ca. 3.5 vol%). The results show the non-linear behavior of the plant, with different transient responses to step change set-point increase and decrease in key plant inputs, and at different loads of the plant.

Figure 8a shows the total stabilization time for lean CO_2 loading L_l at the inlet of the absorber, which ranges from 25 to 45 min in all cases. The results show that the required time for total stabilization increases when the plant is operated at lower loads. As shown in Appendix A (Tables A1 and A2), a general trend was that the dead time θ in the response of L_l to step changes in reboiler duty and rich solvent mass flow rate increases at part-load points. This could be explained by the fact that at lower loads the solvent mass flow rate is smaller (refer to F_{solv} in Table 6), resulting in longer residence times of the solvent through each equipment hold-up, piping, and recycle loop, this is, larger circulation time. This can also explain why dead times are generally larger when decreasing solvent flow rate than when increasing it; refer to Table A2 in Appendix A.
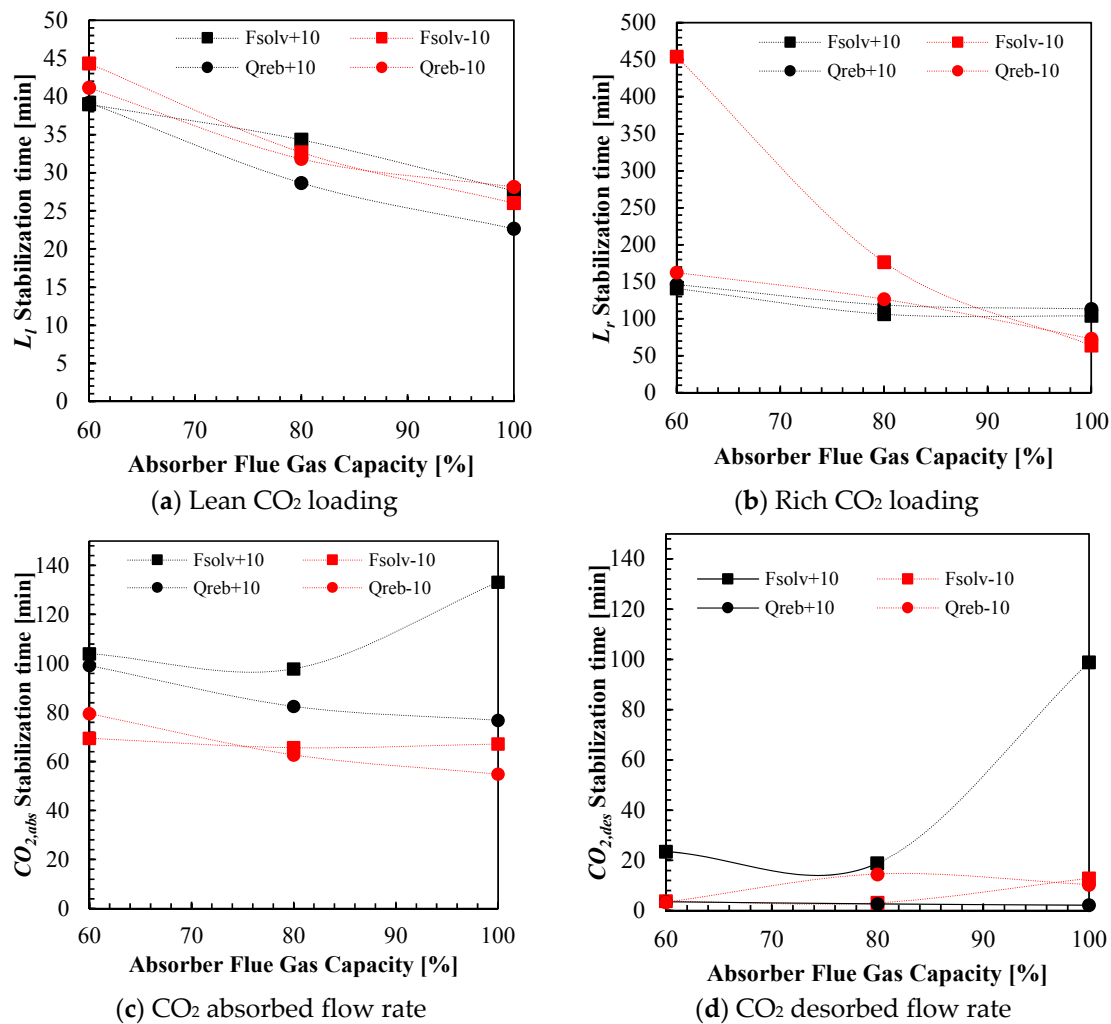
Figure 8. Simulation results. Total stabilization times t_s for open-loop $\pm$ 10% step changes in solvent flow rate and reboiler duty for the process variables (**a**) Lean CO_2 loading L_l; (**b**) rich CO_2 loading L_r; (**c**) CO_2 absorbed $CO_{2,abs}$ and (**d**) CO_2 desorbed $CO_{2,abs}$. Stabilization times are calculated for the response when the plant is operated at three different operating points in terms of flue gas mass flow rate, 100%, 80% and 60% of nominal capacity; refer to Tables 5 and 6.

Figure 8b shows the total stabilization times for rich CO_2 loading L_r at the outlet of the absorber sump. In this case, the stabilization times range from 60 to 450 min. It should be mentioned that the relative change RC in rich CO_2 loading is also small or negligible for the disturbances studied (see Appendix A), due to the fact that the solvent is operated close to its maximum loading capacity of 0.51 mol/mol CO_2 loading. The total stabilization times of the responses of rich CO_2 loading L_r to disturbances in solvent flow rate and reboiler duty are larger at lower plant loads. At 60% flue gas capacity, a very slow response is found in L_r when the solvent flow rate is decreased by a -10% step change; however, the relative change RC of L_r in this process variable is negligible for this plant disturbance; refer to Table A2 in Appendix A.

The total stabilization times for CO_2 absorbed $CO_{2,abs}$ response to disturbances in rich solvent mass flow rate F_{solv} and reboiler duty $\dot{Q}_{reb}$ are shown in Figure 8c. Total stabilization times range from 55 to 135 min. When the rich solvent mass flow rate is increased by 10%, this results in an increase in CO_2 absorbed with a relative change RC of 0.35% to 4.18% (refer to Table A2), due to the increased L/G ratio in the absorber column. However, since the reboiler duty is kept constant, the lean loading will increase (see RC values of L_l in Table A2). Due to the residence time in the hot solvent piping,

lean/rich heat exchanger and lean amine cooler of the recycle loop, it takes time for the solvent to be distributed towards the inlet of the absorber. A dead time in CO_2 lean loading L_l at the inlet of the absorber of 11 to 22 min is observed (see Table A2). This results in it taking a long time for the $CO_{2,abs}$ to stabilize. When the rich solvent mass flow rate is decreased by 10%, it is observed that the CO_2 absorbed $CO_{2,abs}$ decreases (relative change *RC* between −3.14% and −5.59% in Table A2). This is a result of the combination of the reduction in L/G ratio and the decrease in lean loading L_l. $CO_{2,abs}$ requiring time for stabilization (stabilization time of 65 to 69 min). When reboiler duty $\dot{Q}_{reb}$ is increased by 10%, the lean loading L_l is decreased significantly (*RC* ranging from 6.75 to 8.59%), which results in increase of $CO_{2,abs}$ (relative change *RC* of 4.0% to 6.07%). The change in lean loading L_l is observed at the absorber inlet with a dead time of 13 to 23 min (due to circulation time of the solvent in the recycle loop), and the total stabilization time for $CO_{2,abs}$ for increase in reboiler duty ranges from 76 to 99 min. When reboiler duty $\dot{Q}_{reb}$ is decreased by 10%, the solvent lean loading increases (*RC* of 6.63% to 8.46%), resulting in less CO_2 being absorbed. Relatively slower response in $CO_{2,abs}$ to disturbances in solvent flow rate and reboiler duty were found when the PCC was operated at lower loads (55 to 99 min). An exception is found for the case when the solvent flow rate is increased at 100% mass flow rate operating conditions of the plant.

Figure 8d shows the stabilization times for CO_2 desorbed $CO_{2,abs}$. For disturbances in rich solvent flow rate and reboiler duty, the desorbed CO_2 stabilizes slightly faster at lower loads (ranging from 2 to 100 min). In general, it was found that the desorption rate stabilized faster than the absorption rate $CO_{2,abs}$ for the disturbances in solvent flow rate and reboiler duty applied to the process. When solvent flow rate is decreased, this results in smaller L/G ratio in the absorber column and less CO_2 being desorbed in the stripper column. Since the rich CO_2 loading does not change significantly (*RC* in L_r from 0 to 0.08%), the CO_2 desorbed $CO_{2,des}$ stabilizes faster than the CO_2 absorbed (circulation time through the recycle loop is not affecting the stabilization of $CO_{2,abs}$). When the reboiler duty $\dot{Q}_{reb}$ is increased by 10%, the relative change in CO_2 desorbed is large (4 to 6.07% in Table A3), and with fast total stabilization time (2 to 3 min in Table A3). A change in reboiler duty results in a fast response in the produced stripping vapors, which also results in a fast response in CO_2 product flow rate (CO_2 desorbed). The longest stabilization time for CO_2 desorbed is found when the solvent flow rate is increased at 100% operating conditions. It is notable that there is a big difference in total stabilization times for solvent flow rate increase at different loads of the plant.

5.2. Decentralized Control Structures

In this section, four control structures for the TCM DA amine plant were tested via dynamic process model simulations. The scenario considers realistic load changes on the power plant, by changing flue gas flow rate feed to the absorber column. From a control analysis perspective, flue gas flow rate change can be considered as a disturbance applied to the PCC process. A load change event would result in a significant change in flue gas flow rate, at a ramp rate given by GT operation and controls. Fast ramp rates are the goal of power plant operators, since a fast power plant can respond to the variability in costs in a day-ahead power market [7,64]. For a NGCC power plant, a fast ramp rate is considered to be around 10%/min GT load [4,65]. Two tests were considered and simulated:

- Test 1: Ramping down flue gas flow rate from 100 to 70% in 3 min. The transient event starts at $t_0 = 0$ min, and sufficient simulation time is allowed for the plant to reach the new steady-state.
- Test 2: Flue gas flow rate is ramped up from 70 to 100% in 3 min. The transient event starts at $t_0 = 0$ min, and sufficient simulation time is allowed for the plant to reach the new steady-state.

The supervisory or advanced control layer of the TCM DA amine plant has three main degrees of freedom, consisting of set point of flue gas volumetric flow rate F_{gas}, set point of rich pump solvent flow rate F_{solv}, and steam flow rate to feed the reboiler duty $\dot{Q}_{reb}$; refer to FT1, FT5 and FT4, respectively in Figure 1. Under normal and stable operation of the pilot plant at TCM DA, such degrees of freedom

are changed manually by the operators to bring the plant to different operating conditions. If flue gas flow rate is considered to be a disturbance, there are two degrees of freedom left for operation. Note that here we do not consider the degrees of freedom available to the operators in the stabilizing or regulatory control layer, or for other auxiliary operations of the plant, or start-up procedures. Several studies in the literature suggest that keeping the capture ratio *Cap* and a temperature in the stripper column constant can lead to efficient operation of the process for varying loads of the PCC absorber-desorber process [13]. In this analysis, four control structures were tested, as presented in Table 7. All the feedback control loops are PI controllers, and were tuned with the simple internal model control (SIMC) tuning rules [66].

- **Control structure A** uses F_{solv} to control capture ratio at the top of the absorber *Cap* defined by Equation (13) to the set point of 0.85, and reboiler duty $\dot{Q}_{reb}$ to control the solvent temperature at the stripper bottom T_{str} to the set point of 120.9 °C. This control structure has been previously proposed in the literature in different studies including [14,16], where it shows a fast response and the capability to reject disturbances.

- **Control structure B** uses F_{solv} to control the solvent temperature at the stripper bottom T_{str} to the set point of 120.9 °C, and reboiler duty $\dot{Q}_{reb}$ to control capture ratio at the top of the absorber *Cap* to the set point of 0.85. Note that changes in reboiler duty result in a big change in solvent lean CO_2 loading (large relative change *RC*; see Appendix A). A similar version was suggested by Panahi and Skogestad [14], where it was found that this control structure showed similar dynamic behavior, in response to disturbances in flue gas flow rate, compared with a model predictive control scheme (MPC).

- **Control structure C** utilizes solvent flow rate F_{solv} to control the mass-based L/G ratio in the absorber column at the same value as that in the close-to-design-point operating conditions. This control structure has been studied previously in [12,15]. This control loop is implemented via ratio control. In addition, reboiler duty is manipulated to control T_{str} to 120.9 °C. The control structure leads to different final steady-state operating conditions when ramping down the plant load than the other three alternatives.

- **Control structure D** is a modification of control structure A. In this control structure, the solvent flow rate set point is changed via a feed forward (FF) action to control the capture ratio *Cap* at 0.85; in addition, the stripper bottom temperature is controlled by manipulating the reboiler duty. The feed forward controller is implemented by a set-point ramp change in the solvent flow rate with the same total duration as the flue gas flow rate ramp change, to the final value that gives a *Cap* of 0.85 under final steady-state conditions.

Figure 9 shows the simulated time input trajectories during the test with flue gas flow rate reduction. The manipulated variables F_{solv} and $\dot{Q}_{reb}$ are shown for the different control structures evaluated. Figure 10 shows the output trajectories of CO_2 capture ratio *Cap*, desorption ratio *Des*, CO_2 absorbed and CO_2 desorbed for the transient tests of flue gas flow rate reduction. Figure 11 shows the trajectories of lean loading L_l and stripper bottom solvent temperature T_{str} for flue gas flow rate reduction. In addition, Figure 12 shows the simulated time input trajectories during the test with flue gas flow rate increase. Figure 13 shows the output trajectories of CO_2 capture ratio *Cap*, desorption ratio *Des*, CO_2 absorbed and CO_2 desorbed for the transient tests of flue gas flow rate increase, and Figure 14 shows the trajectories of lean loading L_l and stripper bottom solvent temperature T_{str} for flue gas flow rate increase. In order to compare the different control structure performances during transient load change, the total stabilization times of the selected process variables are shown in Table 8. These will indicate how fast the plant achieves stabilization of the different floating (not controlled) process variables when moving from one operating condition to the next one. In addition, three transient performance indicators have been considered and presented in Table 9. Note that, for this analysis auxiliary consumptions of the plant are not considered.
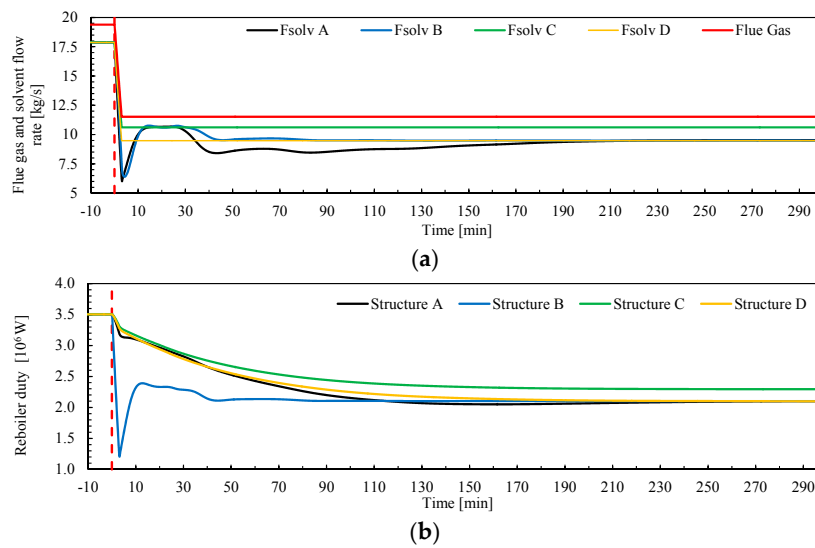
Figure 9. Inputs to the pilot plant during simulations for load change ramp-down (Test 1) from 100 to 70% with a ramp rate of 10%/min reduction in flue gas flow rate, for control structures A, B, C and D. (**a**) Flue gas flow rate (kg/s), as a disturbance, and solvent flow rates (kg/s) of the rich pump as manipulated variables (MVs); (**b**) Reboiler duty (W) as MV. The red vertical dotted line shows when the transient event starts at t_0.
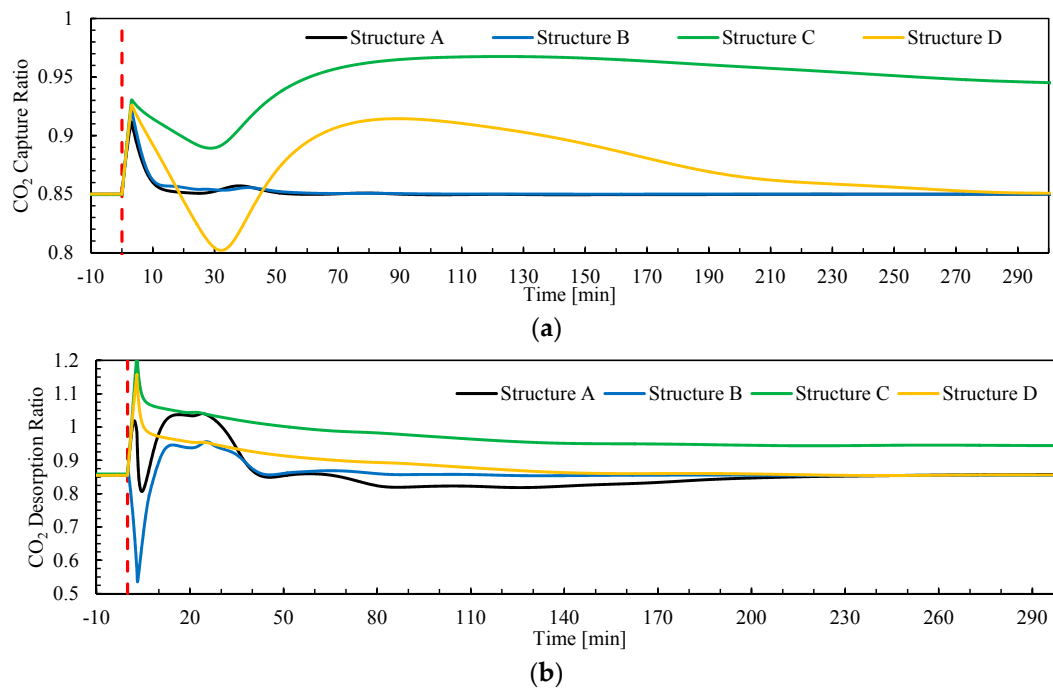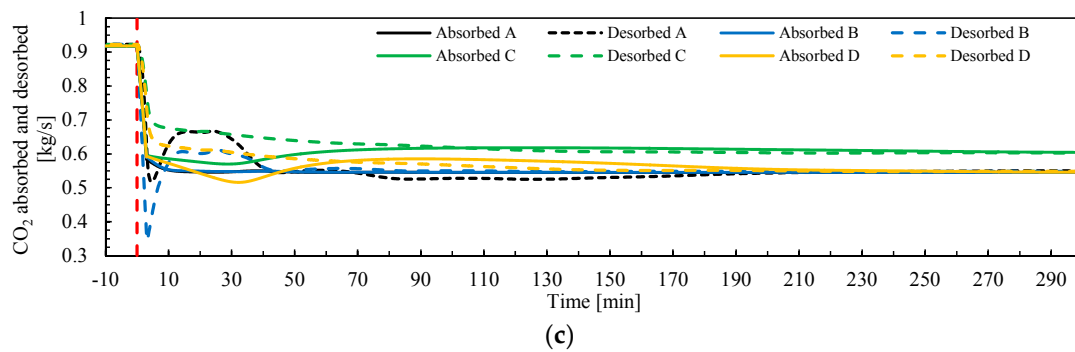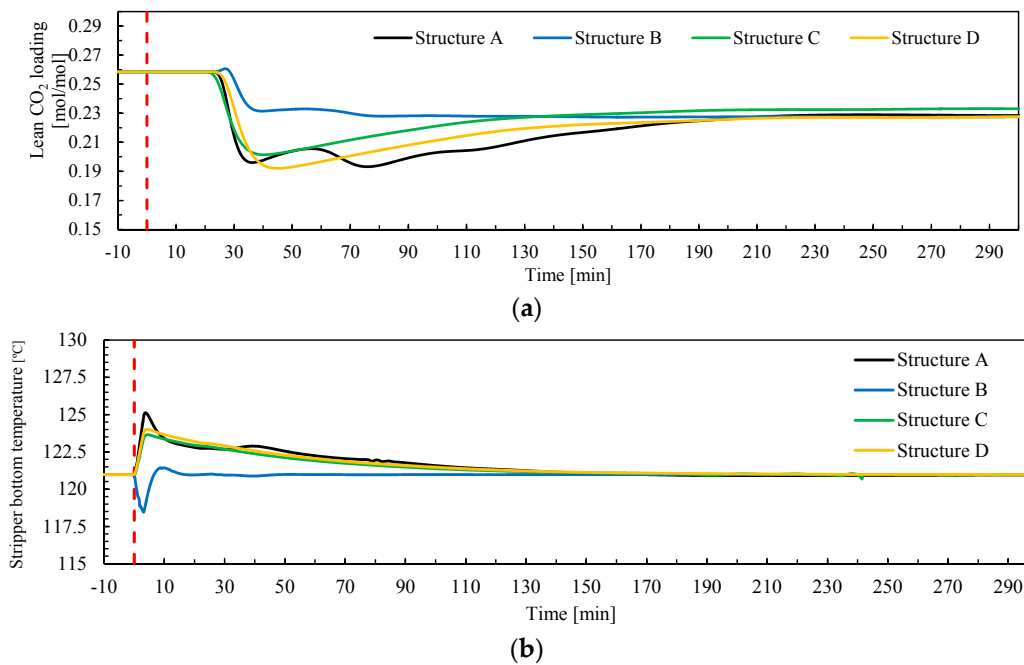

Figure 10. *Cont*.

(c)

Figure 10. Outputs from pilot plant model during simulations for load change ramp-down (Test 1) from 100 to 70% with a ramp rate of 10%/min reduction in flue gas flow rate, for control structures A, B, C and D. (**a**) CO_2 capture ratio *Cap*, as controlled variable (CV); (**b**) CO_2 desorption ratio *Des*; (**c**) CO_2 absorption and desorption rates (kg/s). The red vertical dotted line shows when the transient event starts at t_0.

(a)

(b)

Figure 11. Outputs from pilot plant model during simulations for load change ramp-down (Test 1) from 100 to 70% with a ramp rate of 10%/min reduction in flue gas flow rate, for control structures A, B, C and D. (**a**) Lean CO_2 loading at the inlet of the absorber; (**b**) Stripper bottom temperature as controlled variable (°C). The red vertical dotted line shows when the transient event starts at t_0.
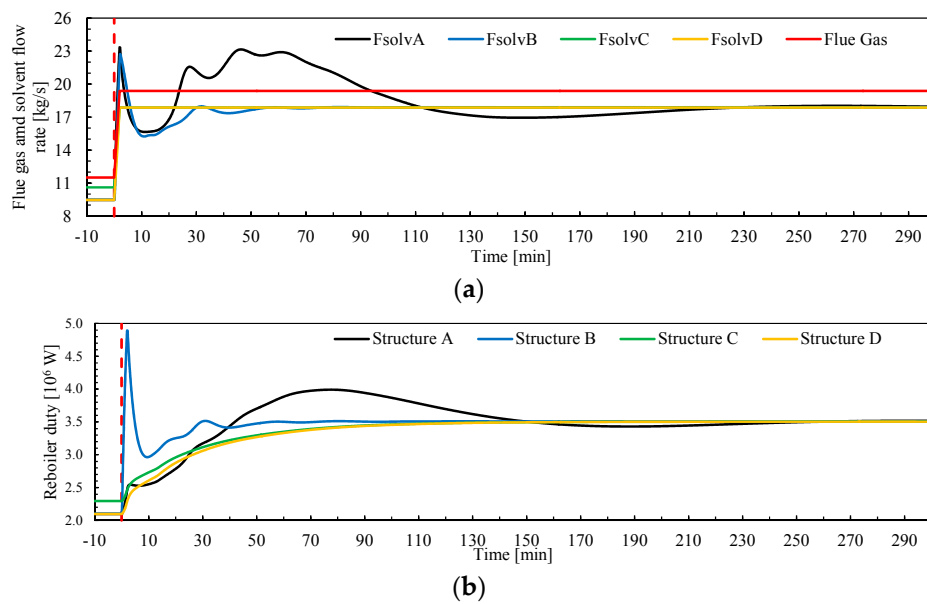
(a)

(b)

Figure 12. Inputs to the pilot plant during simulations for load change ramp-up (Test 2) from 70 to 100% with a ramp rate of 10%/min increase in flue gas flow rate, for control structures A, B, C and D. (**a**) Flue gas flow rate (kg/s), as a disturbance, and solvent flow rates (kg/s) of the rich pump as manipulated variables (MVs); (**b**) Reboiler duty (W) as MV. The red vertical dotted line shows when the transient event starts at t_0.
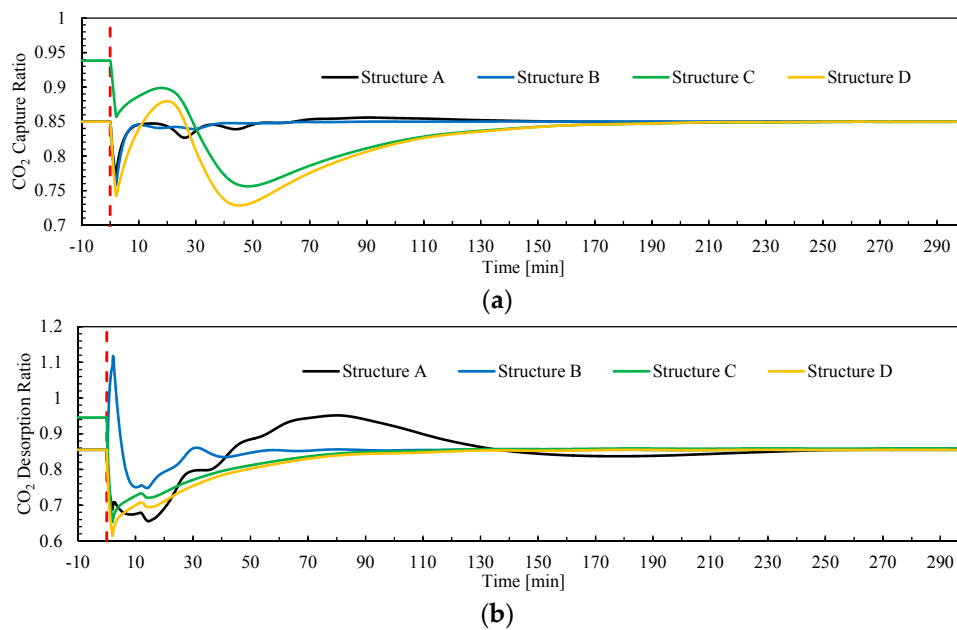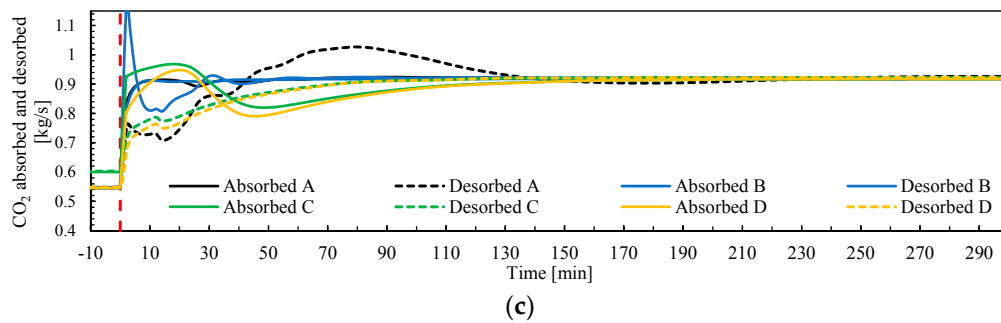

(a)

(b)

Figure 13. *Cont*.

(c)

Figure 13. Outputs from pilot plant model during simulations for load change ramp-up (Test 2) from 70 to 100% with a ramp rate of 10%/min increase in flue gas flow rate, for control structures A, B, C and D. (**a**) CO_2 capture ratio *Cap*, as controlled variable (CV); (**b**) CO_2 desorption ratio *Des*; (**c**) CO_2 absorption and desorption rates (kg/s). The red vertical dotted line shows when the transient event starts at t_0.
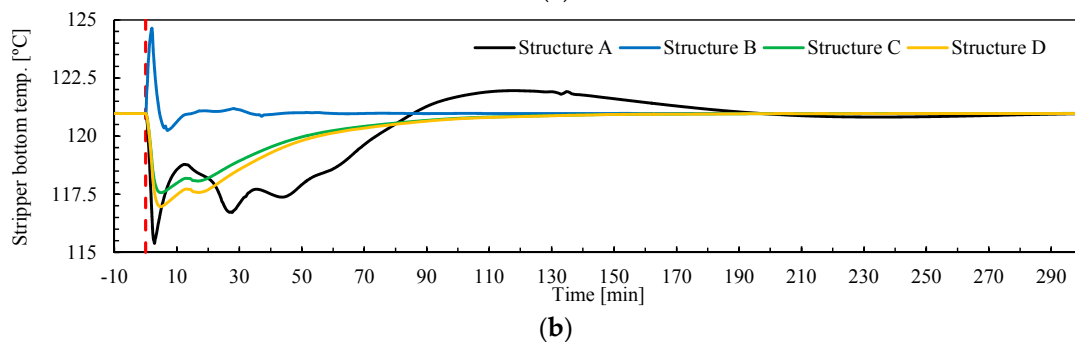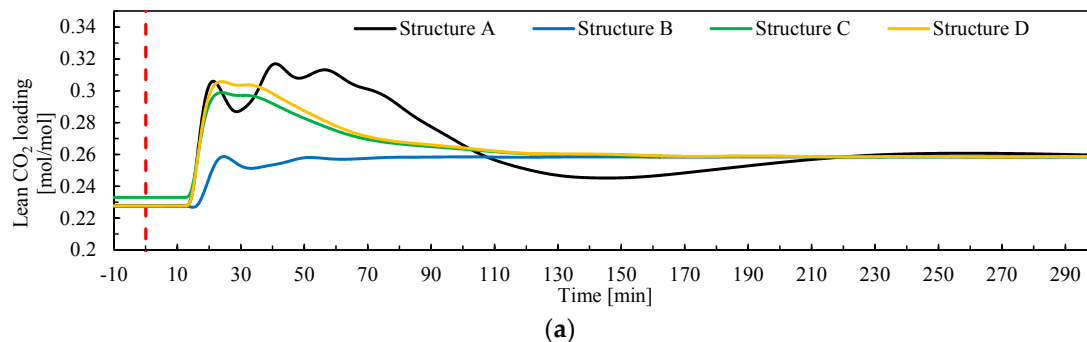

(a)

(b)

Figure 14. Outputs from pilot plant model during simulations for load change ramp-up (Test 2) from 70 to 100% with a ramp rate of 10%/min increase in flue gas flow rate, for control structures A, B, C and D. (**a**) Lean CO_2 loading at the inlet of the absorber; (**b**) Stripper bottom temperature as controlled variable (°C). The red vertical dotted line shows when the transient event starts at t_0.

Table 8. Total stabilization times of the floating process variables for the different control structures, when ramping down the plant $t_{t,down}$ from 100% flue gas mass flow rate to 70%; and when ramping up the plant $t_{t,up}$ from 70% flue gas mass flow rate to 100%.

Control Structure	Process Variable	$t_{t,down}$ (min)	$t_{t,up}$ (min)
A	CO_2 Absorbed	3.3	71.0
	CO_2 Desorbed	36.3	112.7
	L_l	187.7	201.0
B	CO_2 Absorbed	4.0	5.2
	CO_2 Desorbed	35.3	27.5
	L_l	68.2	46.7
C	CO_2 Absorbed	3.6	97.7
	CO_2 Desorbed	56.5	63.7
	L_l	172.2	115.5
D	CO_2 Absorbed	6.2	96.8
	CO_2 Desorbed	50.3	59.2
	L_l	185.0	113.8

Table 9. Simulation results for accumulated reboiler energy consumption Q_{reb} (MJ), accumulated CO_2 emitted $CO_{2,em}$ and accumulated CO_2 captured $CO_{2,cap}$ during the transient event (8 h) for the different control structures A,B, C and D (refer to Table 7), when ramping up and down the plant (between 100% and 70% of flue gas mass flow rate). Static plant refers to an ideal static plant that changes from the initial operating conditions to the final operating conditions instantaneously at time $t = 0$. An integration time of $t_f = 480$ min was utilized to calculate the values for the ideal static plant.

Transient Event	Indicator	Static Plant	A	B	C	D
Ramp down	Q_{reb} (MJ)	60,441	63,353	60,926	69,045	64,046
	$CO_{2,em}$ (tons)	2.66	2.64	2.65	0.96	2.39
	$CO_{2,cap}$ (tons)	15.70	15.76	15.75	17.44	16.01
Ramp up	Q_{reb} (MJ)	100,924	100,898	100,655	98,973	98,667
	$CO_{2,em}$ (tons)	4.49	4.51	4.53	4.77	4.94
	$CO_{2,cap}$ (tons)	26.41	26.39	26.37	26.13	25.96

- **Accumulated reboiler energy input Q_{reb} (MJ)**: see Equation (15). This is calculated by integration of the $\dot{Q}_{reb}$ trajectory under the transient event, from the initial time $t_0 = 0$ min to the final time $t_f = 480$ min (8 h). The final time was defined to ensure that the plant was already under steady-state conditions at the final operating point. This value Q_{reb} represents the main energy consumption of the process during the transient event of load change. In addition, the consumption of an ideal static plant is included for comparison (see Table 9). The ideal static plant is assumed to change from initial to the final steady-state operating conditions instantaneously at time t_0, and would operate until t_f. The static plant value represents the minimum value when ramping down and a maximum value when ramping up.

$$Q_{reb} = \int_{t_0}^{t_f} \dot{Q}_{reb}(t)dt \tag{15}$$

- **Accumulated CO_2 emitted $CO_{2,em}$ (tons)**: see Equation (16). This is calculated by integration of the $\dot{m}_{CO_2}$ trajectory under the transient event, from the initial time $t_0 = 0$ min to the final time $t_f = 480$ min; this represents the CO_2 emitted at the absorber stack. The final time was defined to ensure that the plant was already under steady-state conditions at the final operating point. This measure represents the CO_2 emitted during the transient event of load change.

For comparison, the CO_2 emitted by an ideal static plant is calculated (considered as the maximum value when ramping down and a minimum value when ramping up), shown in Table 9.

$$CO_{2,em} = \int_{t_0}^{t_f} \dot{m}_{CO_2}(t)dt = \int_{t_0}^{t_f} \dot{m}_{depleted}(t) \cdot X_{CO_2}(t)dt \tag{16}$$

- **Accumulated CO_2 captured $CO_{2,cap}$ (tons)**: see Equation (17). This is calculated by integration of the CO_2 absorbed $CO_{2,abs}$ trajectory (Equation (12)) under the transient event, from the initial time $t_0 = 0$ min to the final time $t_f = 480$ min. The final time was defined to ensure that the plant was already under steady-state conditions at the final operating point. This measure represents the CO_2 captured during the transient event of load change. For comparison, the CO_2 captured by an ideal static plant is calculated (considered as the minimum value when ramping down and a maximum value when ramping up), shown in Table 9.

$$CO_{2,cap} = \int_{t_0}^{t_f} \left(F_{gas}(t) \cdot X_{CO_2}(t) - F_{depleted}(t) \cdot X_{CO_{2,out}}(t) \right)dt \tag{17}$$

Figure 10 shows that the CO_2 capture ratio *Cap* had similar trajectories for control structures A and B during Test 1 (flue gas ramp-down), and that *Cap* reached stabilization conditions faster (20–50 min) than control structures C and D (around 270 min). *Cap* had also larger excursions from the set point than when control structures A and B are utilized. The same trends are found for Test 2 with flue gas flow rate ramp-up (Figure 13). When ramping up, control structures C and D stabilize faster (around 160 min) than when ramping down. This showed that the utilization of close-loop feedback control (structures A and B) allows shorter stabilization times to be reached for the controlled variable CO_2 capture ratio *Cap*. The desorption ratio *Des* trajectories in Figure 10 show that the plant requires the shortest stabilization time for this process variable when employing control structure B (around 60 min), followed by control structure A and C (around 200 min). This can be explained by the fact that for a change in reboiler duty the response of CO_2 desorbed has a fast total stabilization time and a large static relative change *RC* (where *RC* ranges from 4 to 6.29% and total stabilization time range from 2.2 to 3.5 min for a +10% step in reboiler duty); refer to Table A3. When it comes to the stabilization time required for *Des* for Test 1, structures C and D presented a poorer performance as the trajectories for *Cap* and *Des* deviate from the set point significantly. For control structure A, *Des* showed slow performance for Test 2 (around 210 min total stabilization time) with significant oscillations around set point; refer to Figure 13.

When ramping down the plant, CO_2 absorbed and CO_2 desorbed require similar stabilization times for control structures A and B (around 3 min for $CO_{2,abs}$ and 36 min for $CO_{2,abs}$), while the control structures C and D require longer stabilization times for CO_2 desorbed (around 50 to 57 min); refer to Table 8. The trajectory of CO_2 lean loading again shows shorter stabilization time for control structure B. This can be explained by the large static relative change *RC* of the response of CO_2 lean loading to changes in reboiler duty (where *RC* ranges from −6.29% to −4.97% and total stabilization time range from 22.7 to 39.2 min for a +10% step in reboiler duty); refer to Table A3. This contributes to the tight control of CO_2 capture ratio *Cap* achieved by control structure B, since the CO_2 lean loading L_l is a key process variable that connects the operation of the stripper and the absorber columns via the recycle loop. In addition, control structure B shows the shortest stabilization times and smaller excursions of the stripper bottom temperature T_{str} (around 15 to 30 min), in Figures 11 and 14.

When the plant load is ramped up from 70 to 100% (Test 2), the control structure B in general showed a faster dynamic performance with significantly shorter stabilization times required for the floating process variables considered (5.2 min for $CO_{2,abs}$, 27.5 min for $CO_{2,abs}$ and 46.7 min for L_l), see Table 9; followed by C, D and A. Note that control structure B presented a faster dynamic performance towards stabilization while ramping up (L_l stabilizes in 46.7 min) than when ramping down the process (L_l stabilizes in 68.2 min). Control structures A, C and D required shorter stabilization

times for CO_2 absorption and CO_2 desorption when ramping down the process load, while CO_2 lean loading stabilized faster when ramping up the plant load; refer to the stabilization time values in Table 9. When the plant is operated under control structure C, the optimum solvent flow rate F_{solv} and lean loading L_l are not reached at the 70% absorber capacity steady-state operating conditions; refer to time >250 min in Figures 9a and 11a, and time <0 min in Figures 12a and 14a. This leads to a higher *Cap* than specified (refer time t > 290 min in Figure 10a and time t < 0 min in Figure 13a), and therefore higher reboiler duty (time t > 290 min in Figure 9b and time t < 0 min in Figure 12b), even though the stripper bottom temperature T_{str} criterion is satisfied.

During the ramp-down transient event of the plant (i.e., period of 8 h from the time change was implemented), the least energy-intensive performance measured by Q_{reb} in Table 9 was observed for control structure B. In addition, this structure shows the largest CO_2 emissions during the transient event, albeit still lower than the ideal static plant. The fast stabilization time of the plant process variables achieved by control structure B provides a transient performance that is the closest to the ideal static plant. Control structures C and D showed the largest CO_2 captured during the transient event. However, when ramping down the plant load, this means that the plant is emitting less CO_2 during the transient event with control structures A, B, C and D than that established by the operational objective and represented by the ideal static plant case. Consequently, when ramping down the plant load, CO_2 emissions will always be lower than those of the equivalent ideal static plant. In addition, the plant is capturing more CO_2 than the ideal static plant. Figure 10a shows how there are periods of time in which the capture ratio *Cap* is above the target of 0.85, leading to more CO_2 being captured than the ideal static plant during the transient event. Control structures A and B showed the largest CO_2 emitted when compared with the ideal static case. Despite control structure A presenting a similar amount of CO_2 emitted during the transient event, it requires a larger amount of energy input during this period than control structure B. Therefore, control structure B shows the best performance in terms of energy consumption and CO_2 emissions during the transient load change event of ramping down the PCC plant load. When ramping up the plant load the most energy-intensive control structure is control structure B. However CO_2 emissions are the lowest, being closer to the minimum established by the static plant. This means that, when ramping up the plant load, CO_2 emissions will always be higher than those of the equivalent ideal static plant. While control structure D is the least energy-intensive process during the transient event of load change increase, it is the control structure with the largest CO_2 emissions during this transient event.

6. Conclusions

The pilot plant data obtained in this work from an MEA campaign at TCM DA amine plant includes ten steady-state operating data sets. The data sets consist of a wide range of steady-state operating conditions of the chemical absorption process in terms of L/G ratio in the absorber column, different absorber packing heights, CO_2 capture ratios, reboiler duty and flue gas flow rate fed to the absorber. The data is considered reliable and valid and can be used for process model validation purposes. In addition, the three transient data sets presented in this work represent transient operation of the pilot plant driven by set-point changes in flue gas flow rate, solvent circulation flow rate and reboiler duty. The transient data sets are considered reliable and suitable for dynamic process model validation purposes, provided that input trajectories can be applied to the dynamic process model.

The validation of the dynamic process model with the steady-state and transient data shows that the process model has a good capability of predicting the steady-state and transient behavior of the plant for a wide range of operating conditions. The validation included in this work proves the capacities of dynamic process modeling applied to large-scale experimental data. The model is considered suitable for studies including transient performance analysis and control structure evaluation studies at the plant scale. In addition, it provides confidence towards using the dynamic process model for analysis of larger-scale PCC plants.

The case study carried out in this work via dynamic process simulations with the validated model shows that, generally, the plant responds more slowly at lower operating loads (the load being defined by the flow rate fed to the absorber). A general trend is observed, in which it takes a longer time to stabilize the main process variables of the pilot plant under open-loop step changes in the main inputs of the process, namely solvent flow rate, flue gas flow rate and reboiler duty. From the process simulations, it is found that, in general, the desorption rate stabilizes faster than the absorption rate for set-point step changes in solvent flow rate and reboiler duty. In addition, $\pm 10\%$ step changes in flue gas flow rate around a given operating point do not cause a large relative change in the main process variables of the process (*RC* ranges from -0.81% to 0.21%).

The evaluation of the decentralized control structures shows that by adding closed-loop controllers on the two main degrees of freedom of the plant—solvent flow rate and reboiler duty—to control two other process variables, including CO_2 capture ratio and stripper bottom solvent temperature, the plant can be stabilized faster and more efficiently under varying loads. The control structure that showed the best performance was control structure B, in which the reboiler duty is manipulated to control CO_2 capture ratio at the inlet of the absorber and the rich solvent flow rate to control the stripper bottom solvent temperature. It was observed that control structure B provides the fastest stabilization times for the main process variables under scenarios when the plant load is ramped down and up, with ramp rates typically found in NGCC power plants with fast-cycling capabilities. When reducing the PCC process load, this control structure is the least energy-intensive of those evaluated in this work. When increasing the plant load, this control structure is the one with the lowest accumulated CO_2 emissions imposed by the process inertia during load-change transient operation.

Author Contributions: Rubén M. Montañés contributed to the selection of experimental data; processed the experimental data; developed the models; carried out the calibration, validation and simulation of the dynamic process models; defined and carried out the case studies; analyzed the results; and wrote the manuscript. Nina E. Flø contributed to the experimental data selection; contributed to the critical analysis of the results; and reviewed the manuscript. Lars O. Nord contributed to the critical analysis of the results; reviewed the manuscript; and supervised the work.

Conflicts of Interest: The authors declare no conflict of interest.

Abbreviations and Symbols

A_{if}	Contact area
AP	Absolute percentage error
Cap	CO_2 capture ratio
CHP	Combined heat and power
CCS	Carbon capture and storage
CO_2	Carbon dioxide
$CO_{2,em}$	CO_2 emitted (kg/s)
c_i	Molar concentration
C_{ef}	Pre-multiplying coefficient
DCC	Direct contact cooler
Des	Desorption ratio
D_{CO2}	Diffusivity of CO_2 in aqueous monoethanolamine
E	Enhancement factor
F	Mass flow rate (kg/s)

FB	Feedback
FC	Flow controller
FF	Feed-forward
FT	Flow transmitter
GA	Gas analyzer
GC	Gas chromatograph
GT	Gas turbine
He_i	Henry's constant
H_2O	Water
HX	Heat exchanger
k_i	Mass transfer coefficient
K_i	Equilibrium constant
LC	Level controller
L_l	Lean CO_2 loading
L_r	Rich CO_2 loading
L/G	Mass-based liquid to gas ratio (kg/kg)
LT	Level transmitter
MAP	Mean absolute percentage error
MEA	Monoethanolamine
MPC	Model predictive control
N_2	Nitrogen
NCCC	National carbon capture center
NGCC	Natural gas combined cycle
O_2	Oxygen
p	Pressure (Pa)
PC	Pressure controller
PCC	Post-combustion CO_2 capture
PT	Pressure transmitter
PZ	Piperazine
$\dot{Q}_{reb}$	Reboiler duty (W)
Q_{reb}	Reboiler energy input (J)
RC	Relative change
SA	Solvent analyzer
SIMC	Simplified internal model control
SRD	Specific reboiler duty (kJ/kgCO_2)
T	Temperature (K)
TC	Temperature controller
TCM DA	CO_2 Technology Cener Mongstad
t_s	Settling time
t_t	Total stabilization time
TT	Temperature transmitter
X	Mass fraction
x_p	Value measured at pilot plant
x_m	Value simulated model
y_∞	Steady-state final value
θ	Dead time
γ_i	Activity coefficient
ΔH_r	Heat of reaction
Δy	Change in process variable
ε-NTU	Effectiveness number of thermal units

Appendix A

Tables A1–A3 show the simulation results in terms of the dead time θ, 10% settling time t_s, total stabilization time t_t and relative change RC %, for the open-loop response to step-changes in the main inputs to the plant. The step changes are applied to the plant when it is operated at three different steady-state operating conditions defined by three different mass flow rate capacities of the absorber column. The inputs are:

- Flue gas mass flow rate ±10% step-change.
- Solvent mass flow rate ±10% step-change.
- Reboiler duty ±10% step-change.

The output process variables studied are:

- CO_2 lean loading L_l (mol/mol).
- CO_2 rich loading L_r (mol/mol).
- CO_2 absorbed $CO_{2,abs}$ (kg/s).
- CO_2 desorbed $CO_{2,abs}$ (kg/s).

Table A1. Open-loop response to ±10% step-changes in flue gas mass flow rate for three different operating points of the pilot plant. Responses in CO_2 lean loading L_l, CO_2 rich loading L_r, CO_2 absorbed, and CO_2 desorbed.

Plant Load	Input Process Variable	F_{gas} +10%				F_{gas} −10%			
		θ (min)	t_s (min)	t_t (min)	RC (%)	θ (min)	t_s (min)	t_t (min)	RC (%)
100%	L_l	40.5	296.5	337.0	0.01	33.5	133.2	166.7	−0.35
	L_r	0.0	41.7	41.7	0.09	19.0	116.3	135.3	−0.76
	$CO_{2,abs}$	0.0	95.2	95.2	0.05	0.0	168.7	168.7	−0.81
	$CO_{2,abs}$	22.2	244.3	266.5	0.04	22.7	128.7	151.3	−0.80
80%	L_l	50.3	260.8	311.2	−0.03	42.7	442.0	484.7	0.04
	L_r	0.0	53.3	53.3	0.21	67.2	117.5	184.7	−0.15
	$CO_{2,abs}$	0.0	61.8	61.8	−0.03	0.0	334.5	334.5	−0.06
	$CO_{2,abs}$	25.5	393.7	419.2	−0.03	23.8	364.7	388.5	−0.06
60%	L_l	51.9	424.9	476.8	−0.03	53.7	318.5	372.2	0.08
	L_r	0.0	96.1	96.1	0.00	0.0	192.8	192.8	−0.05
	$CO_{2,abs}$	0.0	113.7	113.7	−0.05	0.0	141.2	141.2	0.09
	$CO_{2,abs}$	27.7	363.4	391.1	−0.05	25.6	369.9	395.5	0.09

Table A2. Open-loop response to ±10% step-changes in solvent mass flow rate for three different operating points of the pilot plant. Responses in CO_2 lean loading L_l, CO_2 rich loading L_r, CO_2 absorbed, and CO_2 desorbed.

Plant Load	Input Process Variable	F_{solv} +10%				F_{solv} −10%			
		θ (min)	t_s (min)	t_t (min)	RC (%)	θ (min)	t_s (min)	t_t (min)	RC (%)
100%	L_l	11.8	15.8	27.7	8.59	14.5	11.5	26	−7.50
	L_r	14.2	89.7	103.8	−0.10	0	63.83	63.83	0.08
	$CO_{2,abs}$	0.0	133.2	133.2	0.35	0	67.16	67.16	−3.14
	$CO_{2,abs}$	0.0	98.8	98.8	0.35	0	12.83	12.83	−3.15
80%	L_l	15.8	18.5	34.3	7.85	19.5	13.16	32.66	−6.87
	L_r	0.0	106.3	106.3	−0.04	0	176.66	176.66	0.02
	$CO_{2,abs}$	0.0	97.8	97.8	2.09	0	65.66	65.66	−4.38
	$CO_{2,abs}$	0.0	18.8	18.8	2.09	0	3.16	3.16	−4.39
60%	L_l	22.0	17.0	39.0	6.75	27	17.33	44.33	−6.28
	L_r	0.0	141.0	141.0	−0.02	0	454	454	0.00
	$CO_{2,abs}$	0.0	104.0	104.0	4.18	0	69.5	69.5	−5.59
	$CO_{2,abs}$	0.0	23.5	23.5	4.18	0	3.8	3.8	−5.59

Table A3. Open-loop response to ±10% step-changes in reboiler duty for three different operating points of the pilot plant. Responses in CO_2 lean loading L_l, CO_2 rich loading L_r, CO_2 absorbed, and CO_2 desorbed.

Plant Load	Input Process Variable	$\dot{Q}_{reb}$ +10%				$\dot{Q}_{reb}$ −10%			
		θ (min)	t_s (min)	t_t (min)	RC (%)	θ (min)	t_s (min)	t_t (min)	RC (%)
100%	L_l	13.0	9.7	22.7	−6.29	12.7	15.5	28.2	8.46
	L_r	31.8	81.5	113.3	−0.22	29.5	43.3	72.8	0.00
	$CO_{2,abs}$	6.0	70.8	76.8	6.07	5.0	49.8	54.8	−8.48
	$CO_{2,abs}$	0.0	2.2	2.2	6.07	0.0	10.3	10.3	−8.48
80%	L_l	17.0	11.7	28.7	−5.60	17.0	14.8	31.8	7.78
	L_r	40.7	78.0	118.7	−0.03	38.3	88.0	126.3	0.02
	$CO_{2,abs}$	7.8	74.7	82.5	5.19	5.7	57.0	62.7	−7.16
	$CO_{2,abs}$	0.0	2.7	2.7	5.19	0.0	14.5	14.5	−0.05
60%	L_l	23.2	16.0	39.2	−4.97	23.8	17.3	41.2	6.63
	L_r	47.0	99.3	146.3	−0.01	47.8	114.7	162.5	0.00
	$CO_{2,abs}$	9.5	89.6	99.1	4.00	7.5	72.0	79.5	−5.30
	$CO_{2,abs}$	0.0	3.5	3.5	4.00	0.0	3.3	3.3	−5.30

References

1. The International Energy Agency (IEA). *CO_2 Capture and Storage: A Key Carbon Abatement Option*; International Energy Agency: Paris, France, 2008.

2. Singh, A.; Stéphenne, K. Shell Cansolv CO_2 capture technology: Achievement from first commercial plant. *Energy Procedia* **2014**, *63*, 1678–1685. [CrossRef]

3. Laboratory, N.E.T. Petra Nova Parish Holdings. W.A. Parish Post-Combustion CO_2 Capture and Sequestration Project. Available online: https://www.netl.doe.gov/research/coal/project-information/fe0003311-ppp (accessed on 28 September 2017).

4. Hentschel, J.; Babić, U.A.; Spliethoff, H. A parametric approach for the valuation of power plant flexibility options. *Energy Rep.* **2016**, *2*, 40–47. [CrossRef]

5. Mac Dowell, N.; Staffell, I. The role of flexible CCS in the UK's future energy system. *Int. J. Greenh. Gas Control* **2016**, *48*, 327–344. [CrossRef]

6. Gaspar, J.; Jorgensen, J.B.; Fosbol, P.L. Control of a post-combustion CO_2 capture plant during process start-up and load variations. *IFAC-PapersOnLine* **2015**, *48*, 580–585. [CrossRef]

7. Montañés, R.M.; Korpås, M.; Nord, L.O.; Jaehnert, S. Identifying operational requirements for flexible CCS power plant in future energy systems. *Energy Procedia* **2016**, *86*, 22–31. [CrossRef]

8. Johnsson, F.; Odenberger, M.; Göransson, L. Challenges to integrate CCS into low carbon electricity markets. *Energy Procedia* **2014**, *63*, 7485–7493. [CrossRef]

9. Boot-Handford, M.E.; Abanades, J.C.; Anthony, E.J.; Blunt, M.J.; Brandani, S.; Mac Dowell, N.; Fernandez, J.R.; Ferrari, M.-C.; Gross, R.; Hallett, J.P.; et al. Carbon capture and storage update. *Energy Environ. Sci.* **2014**, *7*, 130–189. [CrossRef]

10. Flø, N.E.; Kvamsdal, H.M.; Hillestad, M.; Mejdell, T. Dominating dynamics of the post-combustion CO_2 absorption process. *Comput. Chem. Eng.* **2016**, *86*, 171–183. [CrossRef]

11. Karimi, M.; Hillestad, M.; Svendsen, H.F. Investigation of the dynamic behavior of different stripper configurations for post-combustion CO_2 capture. *Int. J. Greenh. Gas Control* **2012**, *7*, 230–239. [CrossRef]

12. Garðarsdóttir, S.Ó.; Montañés, R.M.; Normann, F.; Nord, L.O.; Johnsson, F. Effects of CO_2-absorption control strategies on the dynamic performance of a supercritical pulverized-coal-fired power plant. *Ind. Eng. Chem. Res.* **2017**, *56*, 4415–4430. [CrossRef]

13. Panahi, M.; Skogestad, S. Economically efficient operation of CO_2 capturing process part i: Self-optimizing procedure for selecting the best controlled variables. *Chem. Eng. Process. Process Intensif.* **2011**, *50*, 247–253. [CrossRef]

14. Panahi, M.; Skogestad, S. Economically efficient operation of CO_2 capturing process. Part II. Design of control layer. *Chem. Eng. Process. Process Intensif.* **2012**, *52*, 112–124. [CrossRef]

15. Montañés, R.M.; GarÐarsdóttir, S.Ó.; Normann, F.; Johnsson, F.; Nord, L.O. Demonstrating load-change transient performance of a commercial-scale natural gas combined cycle power plant with post-combustion CO_2 capture. *Int. J. Greenh. Gas Control* **2017**, *63*, 158–174. [CrossRef]

16. Nittaya, T.; Douglas, P.L.; Croiset, E.; Ricardez-Sandoval, L.A. Dynamic modelling and control of MEA absorption processes for CO_2 capture from power plants. *Fuel* **2014**, *116*, 672–691. [CrossRef]

17. Zhang, Q.; Turton, R.; Bhattacharyya, D. Development of model and model-predictive control of an MEA-based postcombustion CO_2 capture process. *Ind. Eng. Chem. Res.* **2016**, *55*, 1292–1308. [CrossRef]

18. International Energy Agency Greenhouse Gas R&D Programme (IEAGHG). *Evaluation of Process Control Strategies for Normal, Flexible, and Upset Operation Conditions of CO_2 Post Combustion Capture Processes*; July 2016; IEAGHG: Cheltenham, UK, September 2016.

19. Walters, M.S.; Edgar, T.F.; Rochelle, G.T. Regulatory control of amine scrubbing for CO_2 capture from power plants. *Ind. Eng. Chem. Res.* **2016**, *55*, 4646–4657. [CrossRef]

20. Gaspar, J.; Ricardez-Sandoval, L.; Jørgensen, J.B.; Fosbøl, P.L. Controllability and flexibility analysis of CO_2 post-combustion capture using piperazine and MEA. *Int. J. Greenh. Gas Control* **2016**, *51*, 276–289. [CrossRef]

21. Mac Dowell, N.; Shah, N. The multi-period optimisation of an amine-based CO_2 capture process integrated with a super-critical coal-fired power station for flexible operation. *Comput. Chem. Eng.* **2015**, *74*, 169–183. [CrossRef]

22. Flø, N.E.; Kvamsdal, H.M.; Hillestad, M. Dynamic simulation of post-combustion CO_2 capture for flexible operation of the brindisi pilot plant. *Int. J. Greenh. Gas Control* **2016**, *48 Pt 2*, 204–215. [CrossRef]

23. Ceccarelli, N.; van Leeuwen, M.; Wolf, T.; van Leeuwen, P.; van der Vaart, R.; Maas, W.; Ramos, A. Flexibility of low-CO_2 gas power plants: Integration of the CO_2 capture unit with CCGT operation. *Energy Procedia* **2014**, *63*, 1703–1726. [CrossRef]

24. Wellner, K.; Marx-Schubach, T.; Schmitz, G. Dynamic behavior of coal-fired power plants with postcombustion CO_2 capture. *Ind. Eng. Chem. Res.* **2016**, *55*, 12038–12045. [CrossRef]

25. Olaleye, A.K.; Oko, E.; Wang, M.; Kelsall, G. Dynamic modelling and analysis of supercritical coal-fired power plant integrated with post-combustion CO_2 capture. In *Clean Coal Technology and Sustainable Development, Proceedings of the 8th International Symposium on Coal Combustion, Beijing, China, 19-22 July 2015*; Yue, G., Li, S., Eds.; Springer: Beijing, China, 2016; pp. 359–363.

26. Mechleri, E.; Lawal, A.; Ramos, A.; Davison, J.; Dowell, N.M. Process control strategies for flexible operation of post-combustion CO_2 capture plants. *Int. J. Greenh. Gas Control* **2017**, *57*, 14–25. [CrossRef]

27. Mechleri, E.; Fennell, P.S.; Dowell, N.M. Optimisation and evaluation of flexible operation strategies for coal- and gas-CCS power stations with a multi-period design approach. *Int. J. Greenh. Gas Control* **2017**, *59*, 24–39. [CrossRef]

28. Sanchez Fernandez, E.; Sanchez del Rio, M.; Chalmers, H.; Khakharia, P.; Goetheer, E.L.V.; Gibbins, J.; Lucquiaud, M. Operational flexibility options in power plants with integrated post-combustion capture. *Int. J. Greenh. Gas Control* **2016**, *48*, 275–289. [CrossRef]

29. Dutta, R.; Nord, L.O.; Bolland, O. Selection and design of post-combustion CO_2 capture process for 600 MW natural gas fueled thermal power plant based on operability. *Energy* **2017**, *121*, 643–656. [CrossRef]

30. Kvamsdal, H.M.; Jakobsen, J.P.; Hoff, K.A. Dynamic modeling and simulation of a CO_2 absorber column for post-combustion CO_2 capture. *Chem. Eng. Process. Process Intensif.* **2009**, *48*, 135–144. [CrossRef]

31. Gaspar, J.; Cormos, A.-M. Dynamic modeling and absorption capacity assessment of CO_2 capture process. *Int. J. Greenh. Gas Control* **2012**, *8*, 45–55. [CrossRef]

32. Harun, N.; Nittaya, T.; Douglas, P.L.; Croiset, E.; Ricardez-Sandoval, L.A. Dynamic simulation of MEA absorption process for CO_2 capture from power plants. *Int. J. Greenh. Gas Control* **2012**, *10*, 295–309. [CrossRef]

33. Jayarathna, S.A.; Lie, B.; Melaaen, M.C. Amine based CO_2 capture plant: Dynamic modeling and simulations. *Int. J. Greenh. Gas Control* **2013**, *14*, 282–290. [CrossRef]

34. He, Z.; Sahraei, M.H.; Ricardez-Sandoval, L.A. Flexible operation and simultaneous scheduling and control of a CO_2 capture plant using model predictive control. *Int. J. Greenh. Gas Control* **2016**, *48*, 300–311. [CrossRef]

35. Luu, M.T.; Abdul Manaf, N.; Abbas, A. Dynamic modelling and control strategies for flexible operation of amine-based post-combustion CO_2 capture systems. *Int. J. Greenh. Gas Control* **2015**, *39*, 377–389. [CrossRef]

36. Biliyok, C.; Lawal, A.; Wang, M.; Seibert, F. Dynamic modelling, validation and analysis of post-combustion chemical absorption CO_2 capture plant. *Int. J. Greenh. Gas Control* **2012**, *9*, 428–445. [CrossRef]

37. Åkesson, J.; Laird, C.D.; Lavedan, G.; Prölß, K.; Tummescheit, H.; Velut, S.; Zhu, Y. Nonlinear model predictive control of a CO_2 post-combustion absorption unit. *Chem. Eng. Technol.* **2012**, *35*, 445–454. [CrossRef]

38. Bui, M.; Gunawan, I.; Verheyen, V.; Feron, P.; Meuleman, E.; Adeloju, S. Dynamic modelling and optimisation of flexible operation in post-combustion CO_2 capture plants—A review. *Comput. Chem. Eng.* **2014**, *61*, 245–265. [CrossRef]

39. Enaasen, N.; Zangrilli, L.; Mangiaracina, A.; Mejdell, T.; Kvamsdal, H.M.; Hillestad, M. Validation of a dynamic model of the brindisi pilot plant. *Energy Procedia* **2014**, *63*, 1040–1054. [CrossRef]

40. Enaasen Flø, N.; Knuutila, H.; Kvamsdal, H.M.; Hillestad, M. Dynamic model validation of the post-combustion CO_2 absorption process. *Int. J. Greenh. Gas Control* **2015**, *41*, 127–141. [CrossRef]

41. Van De Haar, A.; Trapp, C.; Wellner, K.; De Kler, R.; Schmitz, G.; Colonna, P. Dynamics of postcombustion CO_2 capture plants: Modeling, validation, and case study. *Ind. Eng. Chem. Res.* **2017**, *56*, 1810–1822. [CrossRef] [PubMed]

42. Gaspar, J.; Gladis, A.; Jørgensen, J.B.; Thomsen, K.; von Solms, N.; Fosbøl, P.L. Dynamic operation and simulation of post-combustion CO_2 capture. *Energy Procedia* **2016**, *86*, 205–214. [CrossRef]

43. Dutta, R.; Nord, L.O.; Bolland, O. Prospects of using equilibrium-based column models in dynamic process simulation of post-combustion CO_2 capture for coal-fired power plant. *Fuel* **2017**, *202*, 85–97. [CrossRef]

44. Chinen, A.S.; Morgan, J.C.; Omell, B.P.; Bhattacharyya, D.; Miller, D.C. Dynamic data reconciliation and model validation of a MEA-based CO_2 capture system using pilot plant data. In Proceedings of the 11th IFAC Symposium on Dynamics and Control of Process Systems, Including Biosystems, Trondheim, Norway, 6–8 June 2016.

45. Abdul Manaf, N.; Cousins, A.; Feron, P.; Abbas, A. Dynamic modelling, identification and preliminary control analysis of an amine-based post-combustion CO_2 capture pilot plant. *J. Clean. Prod.* **2016**, *113*, 635–653. [CrossRef]

46. Faber, R.; Köpcke, M.; Biede, O.; Knudsen, J.N.; Andersen, J. Open-loop step responses for the MEA post-combustion capture process: Experimental results from the esbjerg pilot plant. *Energy Procedia* **2011**, *4*, 1427–1434. [CrossRef]

47. Bui, M.; Gunawan, I.; Verheyen, V.; Feron, P.; Meuleman, E. Flexible operation of CSIRO's post-combustion CO_2 capture pilot plant at the AGL Loy Yang power station. *Int. J. Greenh. Gas Control* **2016**, *48*, 188–203. [CrossRef]

48. Tait, P.; Buschle, B.; Ausner, I.; Valluri, P.; Wehrli, M.; Lucquiaud, M. A pilot-scale study of dynamic response scenarios for the flexible operation of post-combustion CO_2 capture. *Int. J. Greenh. Gas Control* **2016**, *48*, 216–233. [CrossRef]

49. De Koeijer, G.M.; Aasen, K.I.; Steinseth Hamborg, E. *Scale-Up and Transient Operation of CO_2 Capture Plants at CO_2 Technology Centre Mongstad*; Society of Petroleum Engineers: Abu Dhabi, UAE, 2014.

50. Gjernes, E.; Pedersen, S.; Cents, T.; Watson, G.; Fostås, B.F.; Shah, M.I.; Lombardo, G.; Desvignes, C.; Flø, N.E.; Morken, A.K.; et al. Results from 30 wt % MEA performance testing at the CO_2 Technology Centre Mongstad. *Energy Procedia* **2017**, *114*, 1146–1157. [CrossRef]

51. Faramarzi, L.; Thimsen, D.; Hume, S.; Maxon, A.; Watson, G.; Pedersen, S.; Gjernes, E.; Fostås, B.F.; Lombardo, G.; Cents, T.; et al. Results from MEA testing at the CO_2 Technology Centre Mongstad: Verification of baseline results in 2015. *Energy Procedia* **2017**, *114*, 1128–1145. [CrossRef]

52. Thimsen, D.; Maxson, A.; Smith, V.; Cents, T.; Falk-Pedersen, O.; Gorset, O.; Hamborg, E.S. Results from MEA testing at the CO_2 Technology Centre Mongstad. Part I: Post-combustion CO_2 capture testing methodology. *Energy Procedia* **2014**, *63*, 5938–5958. [CrossRef]

53. Modelica Association. Available online: https://www.Modelica.Org/ (accessed on 28 September 2017).

54. Modelon. Post-Combustion Capture with Amine Solutions. Available online: http://www.Modelon.Com/industries/energy-process/carbon-capture-and-sequestration/ (accessed on 28 September 2017).

55. Dassault Systems, Dymola. Available online: http://www.3ds.Com/products-services/catia/products/dymola (accessed on 28 September 2017).

56. Prölß, K.; Tummescheit, H.; Velut, S.; Åkesson, J. Dynamic model of a post-combustion absorption unit for use in a non-linear model predictive control scheme. *Energy Procedia* **2011**, *4*, 2620–2627. [CrossRef]

57. Garðarsdóttir, S.Ó.; Normann, F.; Andersson, K.; Prölß, K.; Emilsdóttir, S.; Johnsson, F. Post-combustion CO_2 capture applied to a state-of-the-art coal-fired power plant—The influence of dynamic process conditions. *Int. J. Greenh. Gas Control* **2015**, *33*, 51–62. [CrossRef]

58.　Onda, K.; Takeuchi, H.; Okumoto, Y. Mass transfer coefficients between gas and liquid phases in packed columns. *J. Chem. Eng. Jpn.* **1968**, *1*, 56–62. [CrossRef]

59.　Versteeg, G.F.; Van Dijck, L.A.J.; Van Swaaij, W.P.M. On the kinetics between CO_2 and alkanolamines both in aqueous and non-aqueous solutions. An overview. *Chem. Eng. Commun.* **1996**, *144*, 113–158. [CrossRef]

60.　Holst, J.V.; Versteeg, G.F.; Brilman, D.W.F.; Hogendoorn, J.A. Kinetic study of CO_2 with various amino acid salts in aqueous solution. *Chem. Eng. Sci.* **2009**, *64*, 59–68. [CrossRef]

61.　Böttinger, W. *Nmr-Spektroskopische Untersuchung der Reaktivabsorption von Kohlendioxid in Wässrigen Aminlösungen*; VDI-Verlag: Düsseldorf, Germany, 2006.

62.　Montañés, R.M.; Flø, N.E.; Dutta, R.; Nord, L.O.; Bolland, O. Dynamic process model development and validation with transient plant data collected from an mea test campaign at the CO_2 technology center mongstad. *Energy Procedia* **2017**, *114*, 1538–1550. [CrossRef]

63.　International Energy Agency Greenhouse Gas R&D Programme (IEAGHG). *Operating Flexibility of Power Plants with CCS*; IEAGHG: Cheltenham, UK, June 2012.

64.　Christopher, H.J.; James, K. How to Determine a Unit Ramp Rate (MW/min) for Lowest Total Production Cost. Available online: http://www.heatrate.com/docs/Value-of-Ramp-Rate-1987.pdf (accessed on 28 September 2017).

65.　Genrup, M.; Thern, M. *Ny Gasturbinteknik 2012–2014: Gas Turbine Developments*; Report 2012; ELFORSK: Stockholm, Sweden, 2013.

66.　Skogestad, S.; Grimholt, C. The SIMC method for smooth PID controller tuning. In *Pid Control in the Third Millennium: Lessons Learned and New Approaches*; Vilanova, R., Visioli, A., Eds.; Springer: London, UK, 2012; pp. 147–175.